

# Analyzing Gravitational Waves through Numerical Simulations of Compact Binaries

by

Lorenzo Speri

THESIS  
for the degree of  
BACHELOR OF SCIENCE



Department of Physics  
University of Trento

Supervisor: Bruno Giacomazzo  
July 2018



# Contents

|          |  |           |
|----------|--|-----------|
| <b>1</b> | <b>Introduction</b>  | <b>2</b>  |
| <b>2</b> | <b>From the Einstein's Field Equation<br/>to Gravitational Wave solutions</b>              | <b>4</b>  |
| 2.1      | Linearized Einstein's Field Equation . . . . .   | 4         |
| 2.2      | Gauge Transformations and Radiative Degrees of Freedom . . . . .                           | 7         |
| <b>3</b> | <b>Effects of Gravitational Waves</b>  | <b>10</b> |
| 3.1      | Free Falling Particles and Detection Principles . . . . .                                  | 10        |
| 3.2      | From the Geodesic Deviation Equation to<br>the + and $\times$ Polarization Modes . . . . . | 13        |
| <b>4</b> | <b>Production of Gravitational Waves</b>   | <b>18</b> |
| 4.1      | Solution of the Linearized Einstein's Field Equation . . . . .                             | 18        |
| 4.2      | The Nature of the Gravitational Radiation . . . . .  | 22        |
| <b>5</b> | <b>Numerical Evolution of Compact Binaries</b>   | <b>25</b> |
| 5.1      | Extraction of Gravitational Waves . . . . .  | 25        |
| 5.2      | Binary Black Hole . . . . .  | 27        |
| 5.3      | Binary Neutron Star . . . . .  | 37        |
| <b>6</b> | <b>Conclusions</b>   | <b>42</b> |

# Abstract

The observation of gravitational waves marks the beginning of a new era for studying the Universe. The gravitational radiation plays a crucial role in the theoretical predictions of General Relativity and in the study of violent astrophysical processes, such as compact binary mergers. Therefore, we derive the gravitational wave solutions from the Einstein's field equation and we elucidate the implications of the theoretical predictions using different approaches. Solving the linearized Einstein's field equation, we show that the gravitational radiation produced by a source scales as  $1/r$ .

We present simulations of equal-mass compact binaries with quasi-equilibrium initial conditions. The gravitational waves produced by black hole binaries with six different quasi-equilibrium initial configurations are studied analyzing the differences between the evolution of the systems. We investigate the evolution of a binary neutron star, and we relate the rest mass density evolution to the gravitational wave signal. We explain the communal characteristics of the gravitational waves of black hole and neutron star binaries, and we briefly explain the differences between the nature of such astronomical objects. The theoretical prediction, that the angular frequency of the gravitational wave is twice the orbital angular frequency of the rotating binary, is confirmed by the simulations through a Fourier analysis of the gravitational signal.

The source code and parameters used for the simulations are publicly available, and they are all based on the open-source Einstein Toolkit code. This not only makes it possible to re-run and re-analyze our data, but also enables others to start future researches from this work.

# 1 Introduction

The constancy of the speed of light as measured by observers in different reference frames forces space and time to be mixed into spacetime. When Albert Einstein developed the General Theory of Relativity, he endowed spacetime with curvature and made it dynamical, creating a theory in which all predictions for physical measurements are invariant under changes in coordinates. The speed of light is independent of the observer and it is the speed of causality. Therefore, gravity must be causal as well, and any change to a gravitating source is communicated to a distant observer no faster than the speed of light  $c$ . Such communication of a change in spacetime from a source to an observer leads to the idea that there must exist some notion of gravitational radiation.

From the General Theory of Relativity, it is possible to obtain a tensorial wave equation, which governs the behavior of such gravitational radiation. Therefore, we propose in section(2) the derivation of the gravitational wave solution from the Einstein's field equation using the linearized approximation. Applying the transverse traceless gauge, we find out that the number of radiative degrees of freedom of the general theory of relativity is two. The triumph of theoretical prediction of the gravitational waves (GW) is confirmed by the several experiments.

The first indirect evidence of the existence of gravitational waves was given by Hulse and Taylor [1, 2]. From the study of the orbital decay of a binary pulsar, Hulse and Taylor inferred the emission of gravitational waves, since the two neutron stars were spiraling together at just the rate predicted by general relativity's theory of gravitational radiation reaction.

Subsequently, in 2015, the laser interferometer gravitational wave detector LIGO measured directly the signal of a gravitational wave produced by a binary black hole [3]. And, two years later LIGO-Virgo detector network observed a gravitational-wave signal from the inspiral of two low-mass compact objects consistent with a binary neutron star (BNS) merger [4].

So, in order to understand the basic principles of gravitational wave detectors, in section(3) we study how the gravitational waves perturb free falling particles.

Then, by studying a ring of free falling test particles, we explain the physical interpretation of the two radiative degrees of freedom two polarization states of the GWs.

The gravitational waves are not only the triumph of the General Relativity, but they also give us a completely new method to investigate the nature of binary systems. Binary neutron stars and black holes can imprint a large amount of information in the produced gravitational radiations. However, a thorough study of a gravitational signals needs to be combined with accurate numerical simulations of binary mergers in order to fully understand the link between the gravitational wave production and their sources.

So, firstly, we find a simple theoretical model by solving the linearized Einstein's field equation with the presence of matter in section(4). Then, we apply the obtained solution, the so-called quadrupole formula, for a slowly-moving binary source. And, finally, in the last section(5), by using the open-source computational infrastructure Einstein Tookit[5],

we study the relativistic numerical simulations of compact binaries: binary black holes (BBH) with six different quasi-equilibrium initial configurations and a binary neutron star (BNS) is accomplished. The theoretical prediction from the quadrupole formula, that the frequency of the gravitational wave is twice the orbital angular frequency of the binary, is confirmed in the simulations through a Fourier analysis of the gravitational signal. In addition, we propose a simple gravitational wave extraction method and we also analyze the rest mass density of the binary neutron stars in order to find the relation with the gravitational signal behavior.

## Notation

Throughout, we will use a spacelike signature  $(-, +, +, +)$  and a system of geometrised units in which  $G = c = 1$ , however depending on the need we will also indicate explicitly the speed of light  $c = 299\,792\,458 \text{ m/s}$ , and the Newton constant of gravitation  $G = 6.67408 \times 10^{-11} \text{ N m}^2 \text{ kg}^{-2}$  [6].

We use the Einstein summation convention for repeated indices. Greek letters are used for summing over all the indices from 0 up to 3, whereas latin letters sum only on the spatial indices 1, 2 and 3.

We use the covariant notation of a four-vector

$$x^\sigma = (x^0, x^1, x^2, x^3)$$

or, when we want to aid the comparison with classical Newtonian expression, we use boldface to denote the spatial vectors  $\mathbf{x} = (x, y, z)$  and we rewrite the four-vectors as

$$x^\sigma = (x^0, x^1, x^2, x^3) = (t, \mathbf{x}) = (t, x, y, z)$$

The four-dimensional covariant and partial derivatives will be indicated respectively with  $\nabla_\mu$  and  $\partial_\mu$ .

## Codes, Data and Reproducibility of the simulations

The codes used for the numerical simulations, the scripts for the data analysis and the scripts used to generate the figures are available at the website

<https://github.com/lorenzsp/thesis>

In addition, we have also included the data produced by the simulations in order to reproduce all the results that we have reported in this paper.

In order to reproduce the simulations of the binary black holes and of the binary neutron star, it is possible to download the Einstein Toolkit from the website [7], and use the parameter files at the website <https://github.com/lorenzsp/thesis>.

## 2 From the Einstein's Field Equation to Gravitational Wave solutions

Solving the Einstein's field equation is a mathematically complicated problem, because in general it is difficult to find solutions to the field equations which are non-linear [8]. Therefore, we will obtain the gravitational wave solutions using the weak field linearized approximation and we will discuss the gauge transformations that lead to the two radiative degrees of freedom of the Einstein's field equation.

### 2.1 Linearized Einstein's Field Equation

The Einstein's field equation is a tensor equation that represents how the geometry of spacetime is related to the presence of masses and energy:

$$G_{\mu\nu} \equiv R_{\mu\nu} - \frac{1}{2} g_{\mu\nu} R = 8\pi T_{\mu\nu} \quad (1)$$

On the right hand side we have the energy-momentum tensor  $T_{\mu\nu}$  (or stress-energy tensor), which is interpreted as the flux of four momentum  $p^\mu$  across a surface of constant  $x^\nu$ . On the left hand side the Einstein tensor  $G_{\mu\nu}$  includes a measure of the curvature of spacetime through the Ricci tensor  $R_{\mu\nu}$ , the Ricci scalar  $R = R_{\mu\nu}g^{\mu\nu}$  and the metric  $g_{\mu\nu}$ . In order to solve the Einstein's equation we will make use of the weak field linearized approximation on the metric tensor  $g_{\mu\nu}$  and we will derive the Einstein tensor  $G_{\mu\nu}$  going through the following steps:

- (a) Calculate the Christoffel symbol

$$\Gamma^\alpha_{\beta\gamma} = \frac{1}{2} g^{\alpha\rho} (\partial_\beta g_{\gamma\rho} + \partial_\gamma g_{\rho\beta} - \partial_\rho g_{\beta\gamma}) \quad (2)$$

- (b) Calculate the Riemann curvature tensor

$$R^\alpha_{\beta\gamma\sigma} = \Gamma^\alpha_{\gamma\lambda} \Gamma^\lambda_{\sigma\beta} - \Gamma^\alpha_{\sigma\lambda} \Gamma^\lambda_{\gamma\beta} + \partial_\gamma \Gamma^\alpha_{\sigma\beta} - \partial_\sigma \Gamma^\alpha_{\gamma\beta} \quad (3)$$

- (c) Obtain the Ricci tensor and the Ricci scalar from the Riemann curvature tensor

$$R_{\mu\nu} = R^\alpha_{\mu\alpha\nu} \quad R = \eta^{\mu\nu} R_{\mu\nu} = R^\mu_\mu \quad (4)$$

$G_{\mu\nu}$  and  $T_{\mu\nu}$  are symmetric tensors, since  $g_{\mu\nu}$  is symmetric. So the Einstein's field equation is a set of non-linear second-order partial differential equations with 10 linearly

independent variables.

We show that the equation(1) leads to gravitational wave solutions if we use the **weak field linearized approximation**, which means that we treat the spacetime as nearly flat. Therefore, we assume the metric tensor  $g_{\mu\nu}$  to be equal to the Minkowski metric  $\eta_{\mu\nu} = \text{diag}(-1, +1, +1, +1)$  plus a small metric perturbation  $h_{\mu\nu}$  :

$$g_{\mu\nu} = \eta_{\mu\nu} + h_{\mu\nu} \quad (5)$$

where the metric perturbation is symmetric and  $|h_{\mu\nu}| \ll 1$  for all  $\mu$  and  $\nu$ .

The metric  $g_{\mu\nu}$  is also used to lower and raise indeces, however, in linearized theory we consider only the first order approximation in  $h_{\mu\nu}$ . So, it is possible to raise and lower indeces using the Minkoswian metric  $\eta_{\mu\nu}$ .

Taking into account the mentioned approximations, we follow the itemized procedure to derive the so-called linearized Einstein's field equation.

The Christoffel symbol is obtained keeping up to the first order in the perturbation  $h_{\mu\nu}$

$$\Gamma^\alpha{}_{\beta\gamma} = \frac{1}{2}\eta^{\alpha\rho}(\partial_\beta h_{\gamma\rho} + \partial_\gamma h_{\rho\beta} - \partial_\rho h_{\beta\gamma})$$

Thus, the Riemann curvature tensor becomes

$$\begin{aligned} R^\mu{}_{\beta\gamma\nu} &= \partial_\gamma \Gamma^\mu{}_{\nu\beta} - \partial_\nu \Gamma^\mu{}_{\gamma\beta} \\ &= \frac{1}{2}[\eta^{\mu\rho}(\partial_\gamma \partial_\nu h_{\beta\rho} + \partial_\gamma \partial_\beta h_{\nu\rho} - \partial_\gamma \partial_\rho h_{\beta\nu}) - \eta^{\mu\sigma}(\partial_\nu \partial_\beta h_{\gamma\sigma} + \partial_\nu \partial_\gamma h_{\beta\sigma} - \partial_\nu \partial_\sigma h_{\beta\gamma})] \\ &= \frac{1}{2}(\partial_\gamma \partial_\beta h^\mu{}_\nu - \partial_\gamma \partial^\mu h_{\beta\nu} - \partial_\nu \partial_\beta h^\mu{}_\gamma + \partial_\nu \partial^\mu h_{\beta\gamma}) \end{aligned} \quad (6)$$

where we neglected the first two terms in eq(3) because they are second order terms. Contracting the first and the third indeces we get the Ricci tensor

$$\begin{aligned} R_{\beta\nu} &= \frac{1}{2}(\partial_\mu \partial_\beta h^\mu{}_\nu - \partial_\mu \partial^\mu h_{\beta\nu} - \partial_\nu \partial_\beta h^\mu{}_\mu + \partial_\nu \partial^\mu h_{\beta\mu}) \\ &= \frac{1}{2}(\partial_\mu \partial_\beta h^\mu{}_\nu - \square h_{\beta\nu} - \partial_\nu \partial_\beta h + \partial_\nu \partial^\mu h_{\beta\mu}) \end{aligned}$$

where the trace of the perturbation is defined as  $h = \eta^{\mu\nu} h_{\mu\nu} = h^\mu{}_\mu$ , and the d'Alambertian operator in flat space is  $\square = \partial_\mu \partial^\mu$ .

Contracting again to obtain the Ricci scalar yields

$$\begin{aligned} R &= \frac{1}{2}(\partial_\mu \partial^\nu h^\mu{}_\nu - \square h^\beta{}_\beta - \partial_\beta \partial^\beta h + \partial_\nu \partial^\mu h^\nu{}_\mu) \\ &= \partial_\mu \partial_\nu h^{\mu\nu} - \square h \end{aligned}$$

Therefore the Einstein tensor is

$$G_{\beta\nu} = \frac{1}{2}(\partial_\mu \partial_\beta h^\mu{}_\nu - \square h_{\beta\nu} - \partial_\nu \partial_\beta h + \partial_\nu \partial^\mu h_{\beta\mu} - \eta_{\beta\nu} \partial_\mu \partial_\lambda h^{\mu\lambda} - \eta_{\beta\nu} \square h) \quad (7)$$

If we define the **trace-reversed** perturbation metric

$$\bar{h}_{\mu\nu} = h_{\mu\nu} - \frac{1}{2}h\eta_{\mu\nu} \quad \bar{h} = \bar{h}^{\mu\nu}\eta_{\mu\nu} = -h$$

we can simplify the equation(7). Thus,

$$\begin{aligned} R_{\beta\nu} &= \frac{1}{2} \left( \partial_\mu \partial_\beta \bar{h}^\mu_\nu - \square \bar{h}_{\beta\nu} - \cancel{\partial_\nu \partial_\beta h} + \partial_\nu \partial^\mu \bar{h}_{\beta\mu} + \frac{1}{2} \cancel{\eta_{\nu\mu}} \partial^\mu \cancel{\partial_\beta h} - \frac{1}{2} \eta_{\beta\nu} \square h + \frac{1}{2} \cancel{\eta_{\beta\mu}} \partial_\nu \cancel{\partial^\mu h} \right) \\ &= \frac{1}{2} \left( \partial_\mu \partial_\beta \bar{h}^\mu_\nu - \square \bar{h}_{\beta\nu} + \partial_\nu \partial^\mu \bar{h}_{\beta\mu} - \frac{1}{2} \eta_{\beta\nu} \square h \right) \end{aligned}$$

And contracting the above tensor, we obtain

$$R = \partial_\mu \partial_\beta \bar{h}^\mu_\nu + \frac{1}{2} \eta^{\mu\nu} \partial_\mu \partial_\nu h - \square h = \partial_\mu \partial_\nu \bar{h}^{\mu\nu} - \frac{1}{2} \square h$$

So the Einstein's tensor expressed as a function of  $\bar{h}_{\mu\nu}$  is

$$G_{\beta\nu} = \frac{1}{2} (\partial_\mu \partial_\beta \bar{h}^\mu_\nu - \square \bar{h}_{\beta\nu} + \partial_\nu \partial^\mu \bar{h}_{\beta\mu} - \eta_{\mu\nu} \partial_\mu \partial_\nu \bar{h}^{\mu\nu}) \quad (8)$$

This expression can be further simplified by choosing an appropriate gauge transformation. Using the **Lorenz gauge** condition

$$\partial_\mu \bar{h}^{\mu\nu} = 0 \quad (9)$$

the Einstein's tensor of equation(8) becomes

$$G_{\beta\nu} = \frac{1}{2} (\partial_\beta \partial_\mu \bar{h}^{\mu\alpha} \eta_{\alpha\nu} + \partial_\nu \partial_\mu \bar{h}^{\mu\alpha} \eta_{\alpha\beta} - \eta_{\mu\nu} \partial_\nu \partial_\mu \bar{h}^{\mu\nu} - \square \bar{h}_{\beta\nu}) = -\frac{1}{2} \square \bar{h}_{\beta\nu}$$

The linearized Einstein's field equation is

$$\square \bar{h}_{\beta\nu} = -16\pi T_{\beta\nu} \quad (10)$$

The energy-momentum tensor  $T_{\beta\nu}$  is null in vacuum so the linearized Einstein's equation in vacuum assumes the form of the wave equation in a tensorial form

$$\square \bar{h}_{\beta\nu} = 0 \quad (11)$$

The above equation shows that the trace-reversed metric perturbation propagates as a wave distorting a flat spacetime.

The simplest solution to the linearized Einstein's equation(11) is a plane wave

$$\bar{h}_{\beta\nu} = A_{\beta\nu} \exp(i k_\alpha x^\alpha)$$

where  $A_{\beta\nu}$  is called **amplitude tensor** and it is symmetric, since  $\bar{h}_{\mu\nu}$  is symmetric.

Substitution of the plane wave solution into equation(11) implies that  $k_\alpha k^\alpha = 0$ , so  $k^\alpha$  is a null four vector. Therefore, the plane wave solution is a gravitational wave which travels at the speed of light in the spatial direction  $\mathbf{k} = (k^1, k^2, k^3)/k^0$  and with frequency  $\omega = k^0$ , i.e.  $\bar{h}_{\beta\nu} = A_{\beta\nu} \exp[i(\mathbf{k} \cdot \mathbf{x} - \omega t)]$ . Furthermore, any  $\bar{h}_{\mu\nu}$  satisfying the linearized Einstein's field equation(11) in vacuum describes a **gravitational wave** propagating at the speed of light, and it can be Fourier-expanded as a superposition of plane waves.

## 2.2 Gauge Transformations and Radiative Degrees of Freedom

A **gauge transformation** in linearized theory is defined as a transformation of the perturbation  $h_{\mu\nu}$  into a new metric perturbation  $h'_{\mu\nu}$ , that satisfies

$$h'_{\mu\nu} = h_{\mu\nu} + \partial_\mu \xi_\nu + \partial_\nu \xi_\mu \quad (12)$$

for a given vector field  $\xi^\mu$ . Gauge transformations are particularly important because they leave the Riemann curvature tensor unchanged (up to the first order in  $h_{\mu\nu}$ ), such that, the physical spacetime is unchanged (a simple proof can be found in [9]). The invariance of the curvature under such transformations is analogous to the traditional gauge invariance of electromagnetism.

Assuming that the Einstein's field equation(10) are valid everywhere the metric perturbation  $h_{\mu\nu}$  contains: gauge degrees of freedom; physical, radiative degrees of freedom; and physical, non-radiative degrees of freedom tied to the matter source of the GW.

It is possible to show that the linearized Einstein's equation can be written as 5 Poisson-type quations, plus a wave equation for the transverse-traceless components of the metric perturbation, which represents the radiative degrees of freedom [10, 9].

Nevertheless this procedure will manifestly demonstrate that the radiative degrees of freedom in spacetime are two, it is a cumbersome and long derivation. Instead, we neglect the degrees of freedom tied to the matter setting  $T_{\mu\nu} = 0$  and we analyze only plane wave solutions of equation(11):

$$\bar{h}_{\mu\nu} = A_{\mu\nu} \exp(i k_\alpha x^\alpha)$$

By using the Lorenz gauge and the transverse traceless gauge, we reduce progressively the number degrees of freedom of a plane wave from 10 to 2.

We want now to find the conditions on the parameter  $\xi_\mu$  in order to satisfy the Lorenz gauge condition, that we used in the previous section. The initial metric perturbation  $h_{\mu\nu}$  transforms into  $h'_{\mu\nu}$  if a gauge transformation is used. However, the new trace reversed metric  $\bar{h}'_{\mu\nu}$  transforms as

$$\begin{aligned} \bar{h}'_{\mu\nu} &= h_{\mu\nu} + \partial_\mu \xi_\nu + \partial_\nu \xi_\mu - \frac{1}{2} \eta_{\mu\nu} (h + \partial_\alpha \xi^\alpha + \partial_\alpha \xi^\alpha) \\ \bar{h}'_{\mu\nu} &= \bar{h}_{\mu\nu} + \partial_\mu \xi_\nu + \partial_\nu \xi_\mu - \eta_{\mu\nu} \partial_\alpha \xi^\alpha \end{aligned} \quad (13)$$

Imposing the Lorenz gauge  $\partial_\mu \bar{h}'^{\mu\nu} = \partial_\mu \bar{h}^{\mu\nu} = 0$  we obtain

$$\begin{aligned} \partial_\mu \bar{h}'^{\mu\nu} &= \partial_\mu \bar{h}^{\mu\nu} + \partial_\mu \partial^\mu \xi^\nu + \partial_\mu \partial^\nu \xi^\mu - \partial_\mu \eta^{\mu\nu} \partial_\alpha \xi^\alpha \\ &= 0 + \square \xi^\nu + \partial^\nu \partial_\mu \xi^\mu - \partial^\nu \partial_\alpha \xi^\alpha = 0 \end{aligned}$$

Any metric perturbation  $h_{\mu\nu}$  can therefore be put into a Lorenz gauge by using transformations that satisfy

$$\square \xi_\mu = 0$$

The plane wave  $\xi_\mu = C_\mu \exp[i k_\alpha x^\alpha]$  is a solution of the above equation and it generates a gauge transformation through the four arbitrary constants  $C_\mu$ .

The **Transverse-Traceless (TT) gauge** is the most convenient gauge for the analysis of the gravitational waves, and it is defined for a plane wave by the following conditions:

- a) The Lorenz gauge condition fixes four components of  $A_{\mu\nu}$

$$\partial^\mu \bar{h}_{\mu\nu} = A_{\mu\nu} k^\nu = 0$$

The amplitude tensor  $A_{\mu\nu}$  and the four vector  $k^\mu$  are orthogonal.

- b) Three components of the amplitude tensor can be eliminated selecting  $\xi_\mu = C_\mu \exp[i k_\alpha x^\alpha]$  so that  $A^{\mu\nu} u_\mu = 0$  for some chosen four velocity  $u_\mu$ . Three and not four components are fixed, since one further constraint  $k^\mu A_{\mu\nu} u^\nu$  needs to be satisfied.
- c) One component of the amplitude tensor can be eliminated selecting  $\xi_\mu = C_\mu \exp[i k_\alpha x^\alpha]$  so that  $A_\mu^\mu = 0$ .

This means that we have sufficient freedom to fix the values of 8 components of  $A_{\mu\nu}$  from a), b) and c), hence, reducing the number of independent component from 10 to 2 [11]. Note that  $\bar{h}_{\mu\nu}^{\text{TT}} = h_{\mu\nu}^{\text{TT}}$  from c).

What does the TT gauge tell us about gravitational radiation ?

Let us consider a test particle at rest with four-velocity  $u^\alpha = (1, 0, 0, 0)$  in a nearly flat spacetime. If we orient our spatial coordinate axes so that the a plane gravitational wave is travelling in the positive z-direction (equivalently  $x^3$  direction)  $k^\sigma = (\omega, 0, 0, \omega)$  the transverse traceless conditions becomes

$$\left. \begin{aligned} & A_{\mu 0}^{\text{TT}} \omega + A_{\mu 3}^{\text{TT}} \omega = 0 \\ & A_{0\nu}^{\text{TT}} = 0 \\ & A_{00}^{\text{TT}} + A_{11}^{\text{TT}} + A_{22}^{\text{TT}} + A_{33}^{\text{TT}} = 0 \end{aligned} \right\} \Rightarrow \begin{bmatrix} 0 & 0 & 0 & 0 \\ 0 & A_{11}^{\text{TT}} & A_{12}^{\text{TT}} & 0 \\ 0 & A_{12}^{\text{TT}} & -A_{11}^{\text{TT}} & 0 \\ 0 & 0 & 0 & 0 \end{bmatrix}$$

As a consequence of the transverse traceless gauge the only non-zero component of the metric perturbation  $\bar{h}_{\mu\nu}^{\text{TT}}$  are, respectively, the plus (+) and the cross ( $\times$ ) polarization of the gravitational wave

$$\bar{h}_{11}^{\text{TT}} = -\bar{h}_{22}^{\text{TT}} \equiv h_+$$

$$\bar{h}_{12}^{\text{TT}} = \bar{h}_{21}^{\text{TT}} \equiv h_\times$$

So, the plane wave solution in the TT gauge is:

$$\bar{h}_{\mu\nu}^{\text{TT}} = \begin{bmatrix} 0 & 0 & 0 & 0 \\ 0 & h_+ & h_\times & 0 \\ 0 & h_\times & -h_+ & 0 \\ 0 & 0 & 0 & 0 \end{bmatrix} \quad (14)$$

where we express the real part of the solution with  $x^0 = t$  and  $x^3 = z$  as follow

$$h_+ = A_{11}^{\text{TT}} \cos(\omega(t - z))$$

$$h_\times = A_{12}^{\text{TT}} \cos(\omega(t - z))$$

$h_+$  and  $h_\times$  are the two independent polarizations of a gravitational wave and they completely characterize the gravitational wave solution. We finally found that the radiative degrees of freedom are only two and they are represented by  $h_+$  and  $h_\times$ .

Generally, within any finite vacuum region it is always possible to find a gauge which is locally transverse and traceless [10], that is, a guage which satisfies the following general conditions

$$h_{0\nu}^{\text{TT}} = 0$$

$$\eta^{\mu\nu} h_{\mu\nu}^{\text{TT}} = 0$$

$$\partial_\mu h_{\text{TT}}^{\mu\nu} = 0$$

The transverse traceless gauge does not only simplify the expression of the perturbation metric, but it also gives an important relation between the Riemann curvature tensor and the metric perturbation. Since we have already calculated the Riemann curvature tensor in equation(6) we recall the result taking into account the TT gauge conditions

$$\begin{aligned} R^\mu_{00\sigma} &= \frac{1}{2} (\partial_0 \partial_0 h^{\text{TT}\mu}_\sigma - \partial_0 \partial^\mu h^{\text{TT}}_{0\sigma} - \partial_\sigma \partial_0 h^{\text{TT}\mu}_0 + \partial_\sigma \partial^\mu h^{\text{TT}}_{00}) \\ &= \frac{1}{2} \partial_0 \partial_0 h^{\text{TT}\mu}_\sigma \quad \text{using } h_{\mu 0}^{\text{TT}} = 0 \end{aligned} \quad (15)$$

The above result tells us that the curvature of spacetime is proportional to the 'acceleration' of the gravitational wave. Considering a plane wave we have

$$R^\mu_{00\sigma} = -\frac{1}{2} \omega^2 A^{\text{TT}\mu}_\sigma \cos(\omega(t - z))$$

where  $\omega$  is the frequency of the plane wave. The curvature is proportional to the square of the frequency, in fact we expect a bigger curvature if the wave oscillates more times per second. Nevertheless we considered the simple model of a plane wave, we can say, naively, that the spacetime is more curved if the ripples of the GW are squeezed in a narrow time interval. Analogously, the electromagnetic field of an oscillating electric dipole is proportional to the square of the frequency, in fact we expect a more intense field if the charge oscillates more times per second.

### 3 Effects of Gravitational Waves

We want now to explain the important physical consequences of the theoretical results developed in the previous section. Throughout the next sections we will use the linearized theory of gravitational waves and we consider our metric to be in the TT gauge.

#### 3.1 Free Falling Particles and Detection Principles

In general relativity the trajectory of a free falling particle is described by the **geodesic equation**

$$\frac{d^2x^\beta}{d\tau^2} + \Gamma^\beta_{\mu\nu} \frac{dx^\mu}{d\tau} \frac{dx^\nu}{d\tau} = 0 \quad (16)$$

where the coordinates of the particle are represented  $x^\beta$  and  $\tau$  is the proper time.

We choose a frame in which a test particle is initially at rest, i.e. with initial four-velocity

$$u^\mu = \frac{dx^\mu}{d\tau} = (1, 0, 0, 0)$$

We consider a plane wave in the TT gauge propagating towards the test particle.

Equation(16) can be used to express the initial acceleration of the particle

$$\left( \frac{du^\beta}{d\tau} \right)_0 = -\Gamma^\beta_{00} = -\frac{1}{2}\eta^{\beta\alpha}(\partial_0 h_{\alpha 0} + \partial_0 h_{0\alpha} + \partial_\alpha h_{00}) \quad (17)$$

However, we recall from the TT gauge that

$$h_{0\alpha}^{\text{TT}} = 0 \quad h_{\mu\nu}^{\text{TT}} = \bar{h}_{\mu\nu}^{\text{TT}}$$

for all  $\alpha$ . Hence, the initial acceleration of the particle is zero and a free particle, initially at rest, will remain at rest indefinitely.

In this context "being at rest" means that the coordinates of the particle do not change, so the TT gauge is a good choice of coordinate. As the gravitational waves propagate, the coordinate system moves with the ripples of the spacetime, in order to keep the particle in the initial position. In the TT gauge free falling bodies are not influenced by GWs, and their coordinate separation is constant [12].

However, the proper separation is not constant, so let us calculate it.

Consider two free falling test particles located at  $z = 0$  and separated on the x axis by a coordinate distance  $L_c$ . We still consider a plane wave in the TT gauge propagating in the z direction.

The proper distance between the particles is

$$\begin{aligned} L &= \int_0^{L_c} |g_{\mu\nu} dx^\mu dx^\nu|^{1/2} = \int_0^{L_c} \sqrt{g_{11}} dx = \int_0^{L_c} \sqrt{1 + h_+(t, z=0)} dx \\ &\approx \int_0^{L_c} \left( 1 + \frac{1}{2}h_+(t, z=0) \right) dx = L_c \left( 1 + \frac{1}{2}h_+(t, z=0) \right) \end{aligned}$$

If we had considered two particles on the y axis separated by the same coordinate distance, the proper distance would have been

$$L \approx L_c \left( 1 - \frac{1}{2} h_+(t, z=0) \right)$$

Therefore, recalling the expression of the plus polarization for a plane wave

$$h_+ = A_{11}^{\text{TT}} \cos(\omega(t-z))$$

we notice that the particles along x axis are stretched, whereas the particles along the y axis are squeezed.

The proper distance is stretched by the passing gravitational wave and the two particles oscillate with a fractional length change given by

$$\frac{\delta L}{L} \approx \frac{1}{2} h_+(t, z=0) \quad (18)$$

The proper distance is a very important quantity which has a crucial experimental use. For instance, a laser interferometer gravitational wave detector, that consists of four masses that hang from vibration-isolated supports, compares the difference in the length  $L_1$  and  $L_2$  of two arms as shown in Figure(1). When a gravitational wave passes through the detector, it changes the arm-length difference, thereby an optical system monitors the separations between the masses in such a way that the variations in the output of the photodiode are directly proportional to  $\Delta L = L_1 - L_2$ .

The value of  $\Delta L$  is a composition of the two polarizations of the gravitational wave  $h_+$  and  $h_\times$ , and it also contains terms  $F_+ F_\times$  that weigh the direction of the GW such that

$$\frac{\Delta L}{L} = F_+ h_+(t) + F_\times h_\times(t)$$

One adjusts the reflectivities of the interferometers corner mirrors such that a typical photon travels up and down the cavity of order 200 times before returning to the beam-splitter and being directed into the photodiode. So, the accumulated phase shift in each arm will be

$$\delta\phi \sim 200 \frac{2\pi\Delta L}{\lambda}$$

where  $\lambda$  is the wavelength and  $\Delta L$  is the distance the mirror moves relative to the beam splitter. This phase shift can be measured at the photodiode to an accuracy that is governed by the light's photon shot noise  $\sim 1/\sqrt{N}$ , where  $N$  is the number of photons that enter the interferometer from the laser [13].

## Laser interferometer gravitational wave detector

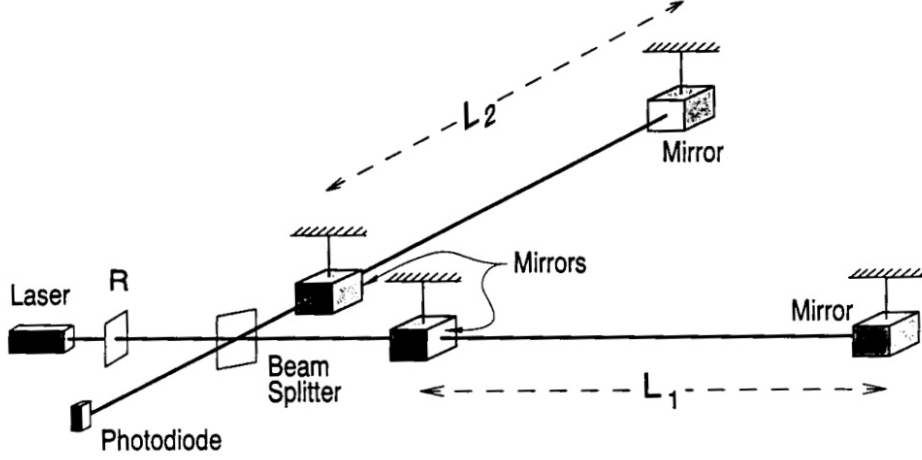


Figure 1: Schematic representation of a laser interferometer gravitational wave detector (Figure from [14]).

In Figure(2), we show the sensitivity curve of the gravitational wave detector as a function of the gravitational strain  $\mathcal{H} \sim \Delta L/L$  and  $f$  the frequency of the gravitational wave.

## Sensitivity of gravitational wave detectors

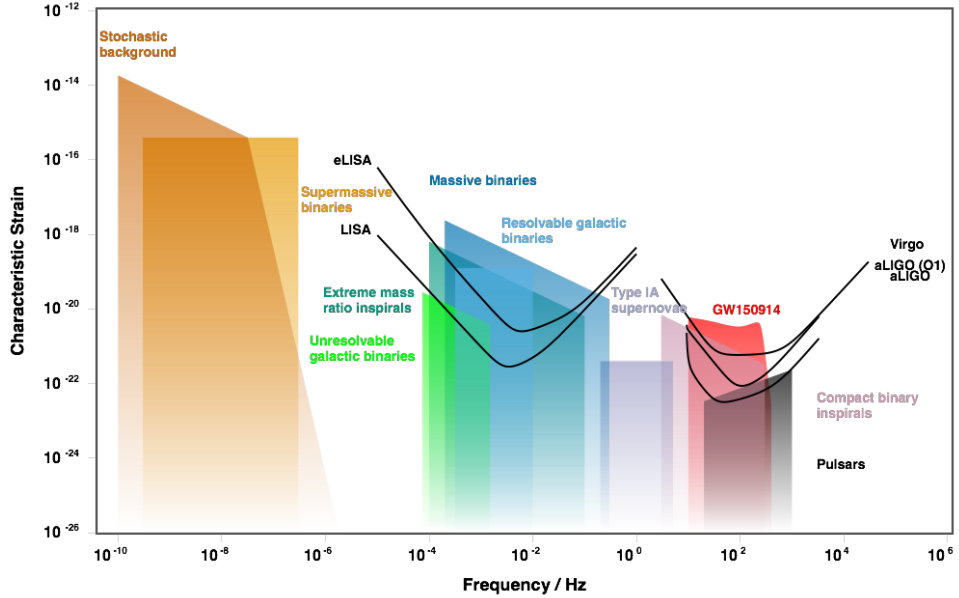


Figure 2: Sensitivity curve of some of the active gravitational wave detectors (Figure from [15]).

## 3.2 From the Geodesic Deviation Equation to the + and × Polarization Modes

Since free-falling bodies obey to the geodesic equation(16), in this section we study the physical effects of the two polarizations plus + and times × of the gravitational waves through relative motions of geodesics.

The **geodesic deviation equation** expresses the relative acceleration between two neighboring geodesics belonging to a one-parameter geodesics  $\gamma_s(\tau)$ :

$$\frac{D^2}{d\tau^2} S^\mu = R^\mu_{\nu\rho\sigma} T^\nu T^\rho S^\sigma \quad (19)$$

where  $S^\mu = \partial x^\mu / \partial s$  is the deviation from the geodesic,  $T^\nu = \partial x^\mu / \partial \tau$  is the tangent to the geodesic and the directional covariant derivative is

$$\frac{D}{d\tau} = \frac{dx^\mu}{d\tau} \nabla_\mu$$

A non-zero acceleration of the deviation between neighbouring geodesics is a signature of spacetime curvature. In fact, geodesic deviation cannot distinguish between a zero gravitational field and a uniform gravitational field. Only tidal gravitational fields give rise to an acceleration in the geodesic deviation.

Let us consider some nearby particles with four-velocities described by a single vector field  $u^\mu$  and separation vector field  $S^\mu$ , the geodesic deviation equation(19) becomes

$$\frac{D^2}{d\tau^2} S^\mu = R^\mu_{\nu\rho\sigma} u^\nu u^\rho S^\sigma \quad (20)$$

The four-velocity vector can be approximated with a unit vector in the time direction plus corrections of order  $h_{\mu\nu}^{\text{TT}}$  and higher, however the Riemann curvature tensor is already a first order in the metric perturbation. Therefore, we ignore the corrections of the four-velocity vector and we approximate  $u^\nu = (1, 0, 0, 0)$ .

Since we have already calculated the Riemann curvature tensor in equation(15), taking into account the TT gauge conditions, we recall the result<sup>1</sup>

$$R^\mu_{00\sigma} = \frac{1}{2} \partial_0 \partial_0 h^{\text{TT}\mu}_{\phantom{\text{TT}\mu}\sigma}$$

In the lowest order approximation the free-falling particles are slowly moving, then we have  $\tau = x^0 = t$ , so the geodesic deviation equation becomes

$$\frac{\partial^2}{\partial t^2} S^\mu = \frac{1}{2} S^\sigma \frac{\partial^2}{\partial t^2} h^{\text{TT}\mu}_{\phantom{\text{TT}\mu}\sigma} \quad (21)$$

---

<sup>1</sup>Since the Riemann curvature tensor is derived from the Christoffel symbol, the two equations (15) (17) may seem incompatible in the TT gauge. However, with the given interpretation they are both correct, for a further discussion look at [16]

### Time evolution of the + polarization



Figure 3: Effect of the  $h_+$  mode on a ring of free-falling test particles at  $\omega t = n\pi/6$  with  $n = 0, \dots, 12$ .

### Time evolution of the $\times$ polarization.



Figure 4: Effect of the  $h_\times$  mode on a ring of free-falling test particles at  $\omega t = n\pi/6$  with  $n = 0, \dots, 12$ .

The above equation is a set of differential equations that can be rewritten using the two polarizations of the metric perturbation (equation(14))

$$\begin{aligned}\frac{\partial^2}{\partial t^2} S^1 &= \frac{1}{2} S^1 \frac{\partial^2}{\partial t^2} h_+ + \frac{1}{2} S^2 \frac{\partial^2}{\partial t^2} h_\times \\ \frac{\partial^2}{\partial t^2} S^2 &= \frac{1}{2} S^1 \frac{\partial^2}{\partial t^2} h_\times - \frac{1}{2} S^2 \frac{\partial^2}{\partial t^2} h_+\end{aligned}$$

These can be solved to yield, to lowest order,

$$\begin{aligned}S^1 &= S^1(t=0) \left( 1 + \frac{1}{2} h_+ \right) + \frac{1}{2} h_\times S^2(t=0) \\ S^2 &= S^2(t=0) \left( 1 - \frac{1}{2} h_+ \right) + \frac{1}{2} h_\times S^1(t=0)\end{aligned}$$

Let us study the effects of the two polarizations  $h_+$  and  $h_\times$  of a gravitational wave, which propagates through the center of a ring of free-falling test particles. So, let us consider a plane wave travelling along the z axis, and let us place a ring of free-falling test particles on the x-y plane with its center in  $(0, 0, 0)$ . The ring is initially parametrized by  $(\cos \theta, \sin \theta)$  with  $\theta \in (0, 2\pi]$  and the separation vector  $S^\mu$  measures the deformation of the ring from its center.

Beginning with the case  $h_\times = 0$  and  $h_+ \neq 0$ , the solutions of the geodesic deviation

equation are

$$S_+^1 = \cos \theta \left( 1 + \frac{1}{2} A_{11}^{\text{TT}} \cos(\omega t) \right) \quad (22)$$

$$S_+^2 = \sin \theta \left( 1 - \frac{1}{2} A_{11}^{\text{TT}} \cos(\omega t) \right) \quad (23)$$

where  $h_+ = A_{11}^{\text{TT}} \cos(\omega t)$  for a plane wave. The time evolution of the ring is shown in Figure(3).

When the plus polarized gravitational wave propagates through the ring, it increases the proper distance between the ring and its center along the x axis when the phase of the wave is close to  $\omega t = 0, 2\pi$ , meanwhile it squeezes the test particles along the y axis. If the phase of the gravitational wave is close to  $\omega t = \pi/2, 3\pi/2$  the ring is stretched along the y axis and the test particles move inwards, therefore, the proper distance from the center of the ring is reduced. As the wave passes, the test particles bounce back and forth in the shape of + as shown in Figure(5a).

On the other hand, the case where  $h_x \neq 0$  and  $h_+ = 0$  yields the geodesic deviation solutions to be

$$\begin{aligned} S_x^1 &= \cos \theta + \frac{1}{2} \sin \theta A_{12}^{\text{TT}} \cos(\omega t) \\ S_x^2 &= \sin \theta + \frac{1}{2} \cos \theta A_{12}^{\text{TT}} \cos(\omega t) \end{aligned}$$

where  $h_x = A_{12}^{\text{TT}} \cos(\omega t)$  for a plane wave. The relationship between these solutions and those for  $h_+ \neq 0$  can be easily found if we rotate the x and y axis through an angle of  $-\pi/4$ , so that the new coordinate axis are

$$x' = \frac{1}{\sqrt{2}}(x - y)$$

$$y' = \frac{1}{\sqrt{2}}(x + y)$$

Then, the geodesic deviations  $S_+$  of equations (22) and (23) with  $h_+ \neq 0$  and  $h_x = 0$  become

$$S'_+{}^1 = (S_+^1 - S_+^2)/\sqrt{2} = \cos(\theta + \pi/4) + \frac{1}{2} \sin(\theta + \pi/4) h_+$$

$$S'_+{}^2 = (S_+^1 + S_+^2)/\sqrt{2} = \sin(\theta + \pi/4) + \frac{1}{2} \cos(\theta + \pi/4) h_+$$

The above equations are similar to those with  $h_+ = 0$  and  $h_x \neq 0$ , in fact the deviations  $S_x^1$  and  $S_x^2$  are nothing but the plus polarization rotated of an angle  $-\pi/4$ . So, in this

case ( $h_+ = 0$  and  $h_\times \neq 0$ ) the ring of test particles bounce back and forth in the shape of  $\times$  as we can see from Figures (4) and (5b).

### + Polarization and $\times$ Polarization

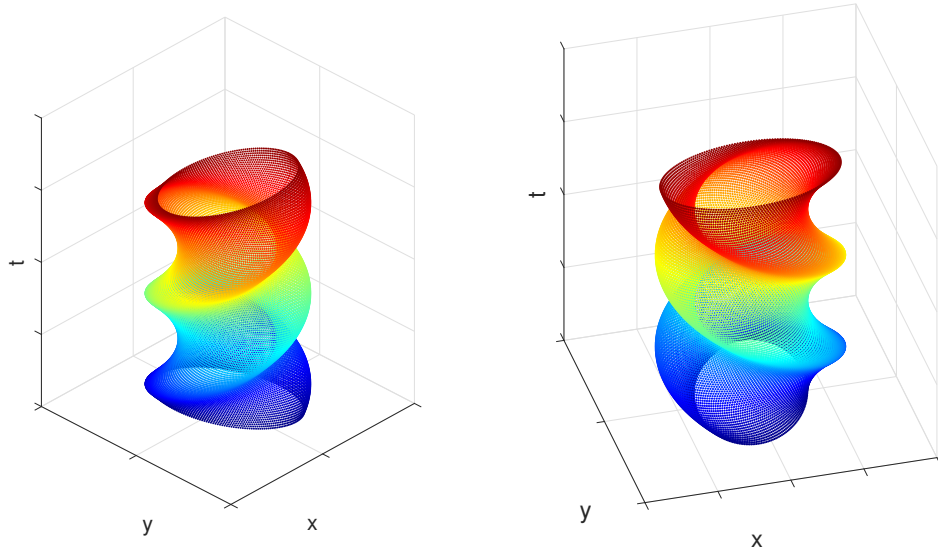


(a) + polarized gravitational wave.

(b)  $\times$  polarized gravitational wave.

Figure 5: Spatial positions occupied by a ring of free-falling test particles disturbed by a gravitational wave.

### Right- and Left-handed circularly polarized modes



(a) Right-handed polarized gravitational wave.

(b) Left-handed polarized gravitational wave.

Figure 6: Time evolution of a ring of free-falling test particles on the x-y plane.

We could consider also right- and left-handed circularly polarized modes by defining

$$h_R = \frac{1}{\sqrt{2}}(h_+ - ih_\times) \quad (24)$$

$$h_L = \frac{1}{\sqrt{2}}(h_+ + ih_\times) \quad (25)$$

The effect of a pure  $h_R$  wave would be to rotate the particles in a right-handed sense and similarly for the left-handed mode  $h_L$  Figure(6). It is important to stress that the particles do not travel around the ring, they just move in little epicycles [9].

It is possible to relate the polarization states of classical gravitational waves to the kinds of particles we would expect to find. The spin of a quantized field is directly related to the transformation properties of that field under spatial rotations. For instance, the electromagnetic field has two independent polarization states, which can be described by vectors in the x-y plane, and they are invariant under a rotation by  $360^\circ$ . Upon quantization, the theory yields the photon, a massless spin-1 particle. The general rule is that the spin  $s$  is related to the angle  $\theta$  under which the polarization modes are invariant by  $s = 360^\circ/\theta$ . Since the gravitational field, whose waves propagate at the speed of light with polarization states invariant under rotations of  $180^\circ$ , should lead to a massless spin-2 particle: the graviton. Despite the fact that we are a long way from detecting such particles, any possible quantum theory of gravity should predict their existence with these properties [9].

## 4 Production of Gravitational Waves

We now want to understand the relation between the gravitational waves and their sources. Therefore, we make several approximations in order to find a solution of the linearized Einstein's field equation(10). In addition, we apply the solution to a slowly moving binary source and we give an estimate of the amplitude of a typical gravitational wave.

We will follow a procedure similiar to [9], however a derivation of the same result can be found also in [17, 10].

### 4.1 Solution of the Linearized Einstein's Field Equation

The production of gravitational radiation depends on the movements of objects in space-time. So far, we have neglected the presence of matter and we solved the linearized Einstein's field equation in vacuum. However, if we want to analyze the relation between sources and gravitational waves we need to consider  $T_{\mu\nu} \neq 0$  and solve equation(10):

$$\square \bar{h}_{\mu\nu} = -16\pi T_{\mu\nu}$$

It is possible to solve this equation using a Green function  $G(x^\sigma - y^\sigma)$ , such that

$$\square_x G(x^\sigma - y^\sigma) = \delta^{(4)}(x^\sigma - y^\sigma) \quad (26)$$

And the general solution is, then, given by

$$\bar{h}_{\mu\nu}(x^\sigma) = -16\pi \int G(x^\sigma - y^\sigma) T_{\mu\nu}(y^\sigma) d^4y \quad (27)$$

$$\square_x \bar{h}_{\mu\nu}(x^\sigma) = -16\pi \int \square_x G(x^\sigma - y^\sigma) T_{\mu\nu}(y^\sigma) d^4y = -16\pi T_{\mu\nu}(x^\sigma)$$

There are two solutions of equation(26): one solution represents a wave travelling forward in time and, the other represents a wave travelling backward in time. The two solutions are called, respectively, retarded and advanced. We are interested in the **retarded Green function**, which represents the accumulated effect of signals received at  $(x^0, x^1, x^2, x^3)$  from a source at  $(y^0, y^1, y^2, y^3)$ :

$$G(x^\sigma - y^\sigma) = -\frac{1}{4\pi|\mathbf{x} - \mathbf{y}|} \delta[|\mathbf{x} - \mathbf{y}| - (x^0 - y^0)] \theta(x^0 - y^0)$$

where have used boldface to denote the patial vectors  $\mathbf{x} = (x^1, x^2, x^3)$  and  $\mathbf{y} = (y^1, y^2, y^3)$ , with norm  $|\mathbf{x} - \mathbf{y}| = [\delta_{ij}(x^i - y^i)(x^j - y^j)]^{1/2}$ . The Heaviside step function  $\theta(x^0 - y^0)$  is 1 when  $x^0 > y^0$ , and zero otherwise.

Plugging the retarded Green function into equation(27) and integrating on the  $y^0$  coordinate we obtain

$$\bar{h}_{\mu\nu}(t, \mathbf{x}) = 4 \int \frac{1}{|\mathbf{x} - \mathbf{y}|} T_{\mu\nu}(t - |\mathbf{x} - \mathbf{y}|, \mathbf{y}) d^3y \quad (28)$$

where  $t = x^0$  and the integration is made over the spatial coordinates. From equation(28) we notice that the metric perturbation is influenced by the matter and energy distribution,  $T_{\mu\nu}$ , at time  $t - |\mathbf{x} - \mathbf{y}|$ . Since the gravitational radiation travels at the speed of light  $c = 1$ , the metric perturbation at  $(t, \mathbf{x})$  is influenced by the radiation that was produced by the source at the retarded time  $t_r = t - |\mathbf{x} - \mathbf{y}|$ .

We have obtained a general solution, however it is possible to derive a more specific formula that will reveal the quadrupole nature of the gravitational radiation, if we make the following assumptions:

- **far field approximation:** the metric perturbation (28) is evaluated at large distances from the source

$$|\mathbf{x} - \mathbf{y}| \approx |x| \equiv r \quad (29)$$

The fractional error of this approximation scales as  $\sim L/r$ , where  $L$  is the size of the source.

- **slowly moving source:** the light traverses the source much faster than the components of the source itself do. Therefore, the source moves at non relativistic speeds.
- **isolated system:** the source of the gravitational radiation is an isolated and compact. We assume that our system and the radiation are not gravitationally influenced by other bodies.

So we rewrite equation(28) using the far field approximation:

$$\bar{h}_{\mu\nu}(t, \mathbf{x}) = \frac{4}{r} \int T_{\mu\nu}(t - r, \mathbf{y}) d^3y$$

Since most of the sources are very far from the detection point, the above result is a very good approximation in most of the cases, and it shows the  $1/r$  dependency of the gravitational wave.

Using the Fourier transform and inverse with respect to time

$$\begin{aligned} \phi(t, \mathbf{x}) &= \mathcal{F}^{-1}[\tilde{\phi}(\omega, \mathbf{x})] \equiv \frac{1}{\sqrt{2\pi}} \int d\omega e^{-i\omega t} \tilde{\phi}(\omega, \mathbf{x}) \\ \tilde{\phi}(\omega, \mathbf{x}) &= \mathcal{F}[\phi(t, \mathbf{x})] \equiv \frac{1}{\sqrt{2\pi}} \int dt e^{i\omega t} \phi(t, \mathbf{x}) \end{aligned}$$

applied to the metric perturbation

$$\begin{aligned}
\mathcal{H}_{\mu\nu}(\omega, t) &\equiv \mathcal{F}[\bar{h}_{\mu\nu}(t, \mathbf{x})] = \frac{1}{\sqrt{2\pi}} \int e^{i\omega t} \bar{h}_{\mu\nu}(t, \mathbf{x}) dt \\
&= \frac{4}{\sqrt{2\pi}} \int e^{i\omega t} \frac{T_{\mu\nu}(t_r, \mathbf{y})}{r} dt d^3y \\
&= \frac{4}{\sqrt{2\pi} r} \int e^{i\omega(t_r+r)} T_{\mu\nu}(t_r, \mathbf{y}) dt_r d^3y \\
&= \frac{4e^{i\omega r}}{r} \int \mathcal{T}_{\mu\nu}(\omega, \mathbf{y}) d^3y
\end{aligned} \tag{30}$$

where we used a change of variable and we defined the Fourier transform of the energy momentum tensor as  $\mathcal{T}_{\mu\nu} \equiv \mathcal{F}[T_{\mu\nu}]$ .

The Lorenz gauge condition  $\partial_\mu \bar{h}^{\mu\nu} = 0$  in the Fourier space becomes

$$\begin{aligned}
\mathcal{F}[\partial_0 \bar{h}^{0\nu} + \partial_j \bar{h}^{j\nu}] &= 0 \\
\mathcal{H}^{0\nu} &= \frac{i}{\omega} \partial_j \mathcal{H}^{j\nu}
\end{aligned}$$

As a consequence, we only need to calculate the spacelike components  $\mathcal{H}^{j\nu}$ . We set  $\nu = k$  in order to find  $\mathcal{H}^{0k}$  from  $\mathcal{H}^{jk}$ , afterwards we use  $\mathcal{H}^{k0}$  to get  $h^{00}$ . The integration by parts of the spacelike components of equation(30) is

$$\int \mathcal{T}^{jk} d^3y = \int \partial_m (\mathcal{T}^{mk} y^j) d^3y - \int \partial_m (\mathcal{T}^{mk}) y^j d^3y$$

Since we assumed that the source is isolated, the first term, which is a surface integral, vanishes. Whereas, the conservation of the energy-momentum tensor  $\partial_\mu T^{\mu\nu} = 0$  yields in the Fourier space

$$-\partial_m (\mathcal{T}^{mk}) = i\omega \mathcal{T}^{0k}$$

Notice that the conservation of the energy-momentum tensor is a very strong assumption, because the motion of bodies is governed by non-gravitational interactions. However, and remarkably, the result depends only on the sources motion and not on the forces acting

on them [18]. Thus,

$$\begin{aligned}
\int \mathcal{T}^{jk}(\omega, \mathbf{y}) d^3y &= i\omega \int y^j \mathcal{T}^{0k} d^3y \\
\text{symmetry of } \mathcal{T}_{kl} &\rightarrow = \frac{i\omega}{2} \int (y^j \mathcal{T}^{0k} + y^k \mathcal{T}^{0j}) d^3y \\
\partial_l(y^k y^j \mathcal{T}^{0l}) = \delta_l^k y^j \mathcal{T}^{0l} + \delta_l^j y^k \mathcal{T}^{0l} + y^k y^j \partial_l \mathcal{T}^{0l} &\rightarrow = \frac{i\omega}{2} \int [\partial_l(y^k y^j \mathcal{T}^{0l}) - y^k y^j \partial_l \mathcal{T}^{0l}] d^3y \\
\partial_l \mathcal{T}^{0l} = \partial_l \mathcal{T}^{l0} = -i\omega \mathcal{T}^{00} &\rightarrow = -\frac{\omega^2}{2} \int y^k y^j \mathcal{T}^{00}(\omega, \mathbf{y}) d^3y
\end{aligned}$$

Then, equation(30) becomes

$$\begin{aligned}
\mathcal{H}_{kj} &= -\frac{4e^{i\omega r}}{r} \frac{\omega^2}{2} \int y^k y^j \mathcal{T}^{00}(\omega, \mathbf{y}) d^3y \\
\mathcal{F}\left[\frac{\partial^2 T^{00}}{\partial t^2}\right] = -\omega^2 \mathcal{F}[T^{00}] &\rightarrow = \frac{2}{r} \int y^k y^j \mathcal{F}\left[\frac{\partial^2}{\partial t^2} T^{00}(t_r, \mathbf{y})\right] d^3y \\
&= \mathcal{F}\left[\frac{2}{r} \frac{\partial^2}{\partial t^2} \left(\int y^k y^j T^{00}(t_r, \mathbf{y}) d^3y\right)\right]
\end{aligned}$$

Applying the inverse Fourier-transform to the above result, we obtain the original metric perturbation

$$\bar{h}_{kj} = \frac{2}{r} \frac{d^2}{dt^2} I_{kj}(t_r) \quad (31)$$

where we define the **quadrupole moment tensor**

$$I_{kj}(t) = \int y_k y_j T^{00}(t, \mathbf{y}) d^3y \quad (32)$$

To complete the derivation we need to express the metric perturbation in the TT gauge, so we must make the right hand side of equation(31) traceless and transverse.

We begin by introducing the spatial projection tensor

$$P_{ij} = \delta_{ij} - n_i n_j \quad (33)$$

which projects the components of a tensor (with rank 2) into a surface orthogonal to the unit vector  $n^i$

$$(P_{ij} X^{il}) n^j = X^{jl} n_j - n_i n_j X^{il} n^j = 0$$

We can use the **projection tensor** to construct the transverse-traceless version of a symmetric spatial tensor  $X_{ij}$  via

$$X_{ij}^{TT} = \left( P_i^k P_j^l - \frac{1}{2} P_{ij} P^{kl} \right) X_{kl} \quad (34)$$

where the first and second terms make the tensor, respectively, transverse and traceless. In addition, we define the **reduced quadrupole moment tensor** as

$$\mathcal{I}_{kj} = I_{kj} - \frac{1}{3}\delta_{kj}I \quad \text{where } I = \eta^{lm}I_{lm} = I_m^m \quad (35)$$

which is traceless, and, for  $T^{00} = \rho$ , it assume the expression

$$\mathcal{I}_{kj} = \int \rho(\mathbf{y}) \left( y_k y_j - \frac{1}{3}\delta_{kj}y^l y_l \right) d^3y$$

We now have all the concepts to write down the **quadrupole formula**

$$h_{ij}^{\text{TT}} = \frac{2}{r} \frac{d^2 \mathcal{I}_{kl}(t_r)}{dt^2} \left( P_i^k P_j^l - \frac{1}{2} P_{ij} P^{kl} \right) \quad (36)$$

which represents the metric perturbation of equation(31) in the TT gauge, since  $h_{\mu\nu}^{\text{TT}} = \bar{h}_{\mu\nu}^{\text{TT}}$ .

Equation(36) represents a general solution of the linearized Einstein's field equation, and it shows that the gravitational wave scales as  $\sim 1/r$ .

The quadrupole formula cannot be used for a black hole because within the Schwarzschild radius of a black hole there is a singularity, which leads to an infinite density.

## 4.2 The Nature of the Gravitational Radiation

The quadrupole formula (36) and its derivation gives a first insight into the properties of the gravitational waves and their sources.

Firstly, the gravitational radiation has a **quadrupolar nature**, because the GW produced by an isolated nonrelativisitic object is proportional to the second derivative of the reduced quadrupole moment of the energy density.

We justify qualitatively the quadrupole nature of the GWs making an analogy with the electromagnetism. Let us define the gravitational analogue of the dipole moment: **mass dipole moment**

$$\mathbf{D} = \sum_i m_i \mathbf{x}_i \quad (37)$$

where the  $m_i$  is the rest mass and  $\mathbf{x}_i$  is the spatial position of particle  $i$ .

In the electromagnetic radiation, the leading contribution to the comes from the changing dipole moment. However, the first derivative of the mass dipole moment is the total linear momentum

$$\frac{d\mathbf{D}}{dt} = \sum_i m_i \frac{d\mathbf{x}_i}{dt} = \mathbf{p}$$

Since the total linear momentum is conserved, there can be no mass dipole radiation from any source.

Similarly, the gravitational analogue of the magnetic dipole moment is

$$\mu = \sum_i \mathbf{x}_i \times \left( m_i \frac{d\mathbf{x}_i}{dt} \right) = \mathbf{J}$$

where  $\mathbf{J}$  is the total angular momentum of the system. Since the total angular momentum is conserved, there can be no dipole radiation of any sort from a gravitational source. So, the quadrupole moment is the first possible moment which can contribute to the production of GWs.

We now study the GW-emission of a binary system in circular orbit with radius  $R$ . We assume that two equal-mass stars are orbiting far from each others with an angular frequency  $\omega$  and they can be treated as point particles on the  $x^1 - x^2$  plane. Thus,

$$T^{00}(t, \mathbf{x}) = M\delta(x^3)[\delta(x^1 - R\cos\omega t)\delta(x^2 - R\sin\omega t) + \delta(x^1 + R\cos\omega t)\delta(x^2 + R\sin\omega t)]$$

The motion of the system is studied using the Newtonian approximations, so using the Kepler third law we obtain the link between the angular frequency and the radius of the orbit:

$$\omega^2 a^3 = M_T G \quad \rightarrow \quad \omega = \left( \frac{M}{4R^3} \right)^{1/2}$$

where we used as total mass of the system  $M_T = 2M$ , semi-major axis  $a = 2R$  and  $G = 1$ . The quadrupole moment tensor (32) becomes

$$I_{ij}(t) = 2MR^2 \begin{bmatrix} \cos^2\omega t & \cos\omega t \sin\omega t & 0 \\ \cos\omega t \sin\omega t & \sin^2\omega t & 0 \\ 0 & 0 & 0 \end{bmatrix}$$

Then, the reduced quadrupole moment (35) is easily found to be

$$\mathcal{I}_{ij}(t) = 2MR^2 \begin{bmatrix} \cos^2\omega t - 1/3 & \cos\omega t \sin\omega t & 0 \\ \cos\omega t \sin\omega t & \sin^2\omega t - 1/3 & 0 \\ 0 & 0 & -1/3 \end{bmatrix}$$

Taking the second derivative of the above tensor and using the projection tensor with  $n_j = \delta_{j3} \rightarrow \mathbf{n} = (0, 0, 1)$ :

$$P_{jk} = \delta_{jk} - n_j n_k$$

we obtain the gravitational wave through the the quadrupole formula(36):

$$h_{ij}^{\text{TT}} = \frac{8GM R^2 \omega^2}{c^4 r} \begin{bmatrix} -\cos 2\omega t_r & -\sin 2\omega t_r & 0 \\ -\sin 2\omega t_r & \cos 2\omega t_r & 0 \\ 0 & 0 & 0 \end{bmatrix}$$

where we inserted  $G$  and  $c$  in order to give an estimates of the coefficient, and  $t_r = t - r/c$  ( $r = z$  in this case).

Two remarkable aspects of the above formula are that the **gravitational wave has an angular frequency that is twice the orbital angular frequency at which the system rotates**, and  $h_{+}^{\text{TT}} = i h_{\times}^{\text{TT}}$  so the wave is circularly polarized.

Let us now give an order-of-magnitude estimate of the amplitude of the gravitational wave, using the coefficient

$$\mathcal{H} = \frac{8GM R^2 \omega^2}{c^4 r}$$

We assume the two objects to be separated by a distance  $R$  equal three times their Schwarzschild radii  $r_s = 2GM/c^2$ . In addition, if the two objects have approximately the mass of the Sun  $M = M_{\odot} = 2 \times 10^{30}\text{kg}$  and they rotate with an angular frequency given by the Kepler's third law  $\omega = \sqrt{GM/(4R^3)}$ , we have

$$\frac{G}{c^4} \approx 8.26 \times 10^{-45}\text{kg}^{-1}\text{s}^2\text{m}^{-1}$$

$$r_s \approx 2.95 \times 10^3 \text{ m}$$

$$R = 3r_s \approx 8.86 \times 10^3 \text{ m}$$

$$\omega \approx 6.9 \times 10^3 \text{s}^{-1}$$

Plugging into  $\mathcal{H}$  and considering the source at the a cosmological distance  $r \approx 100 \text{Mpc} \approx 3.09 \times 10^{24}\text{m}$  we have

$$\mathcal{H} \approx 1.6 \times 10^{-22}$$

Altough we used Newtonian formulae in a regime where the GR becomes to be important, we obtained a reasonable estimate of the gravitational wave amplitude.

Taking into account the discussion we made in section(3.1), if an interferometer of length  $L = 4 \text{ km}$  was affected by a gravitational wave with intensity  $\mathcal{H}$ , the stretching in the arm-length would be of order

$$\delta L \approx L \mathcal{H} \approx 6.38 \times 10^{-19} \text{ m}$$

and the laser light with wavelength  $\lambda = 10^{-6}\text{m}$  would acquire a phase shift

$$\delta\phi = 100 \frac{4\pi}{\lambda} \delta L \approx 8.02 \times 10^{-10}$$

## 5 Numerical Evolution of Compact Binaries

In the linearized approximation, where gravitational fields are weak and velocities are nonrelativistic, we showed that it is straightforward to derive a relationship between the matter dynamics and the emission of gravitational waves, thus obtaining the quadrupole formula. However, the strongest gravitational-wave signals come from highly compact systems that evolve at relativistic speeds, where the linearized assumptions do not apply. Therefore, gravitational-wave detectors find more likely an event which has a powerful signals. Thus, it is important to be able to calculate gravitational-wave emission accurately for processes such as black hole or neutron star inspiral and merger. Such problems cannot be solved analytically and instead are modeled by numerical relativity to compute the gravitational field near the source [11].

In this section we study the gravitational-wave signals obtained from numerical simulations of compact binaries, using the Einstein Toolkit [5, 7, 19], an open-source computational infrastructure for numerical relativity based on Cactus Framework [20].

The Cactus framework is a general framework for the development of modular applications, wherein programs are split into components (called thorns) with clearly defined dependencies and interactions. Thorns are typically developed independently and do not directly interact with each other [21]. Cactus simulations require an executable to be compiled, and this executable has one mandatory argument: a parameter file. The parameter file is a simple text file, containing the desired settings within the simulation, it is used not only to set up the initial conditions and the necessary thorns for the simulation, but also to choose outputs and their format.

A thorough description of the numerical methods used to perform the simulations can be found here [5]. We do not analyze the algorithms of the Einstein Toolkit, we only state the initial conditions of simulations and we briefly mention the used thorns. The purpose of the following sections is to study the gravitational-wave signals of binaries black holes (BBH) and neutron stars (BNS).

### 5.1 Extraction of Gravitational Waves

Firstly, we define the **gravitational wave strain** as

$$h(t) \equiv h_+ + i h_\times \quad (38)$$

Using the thorn `WeylScal4`, the Einstein Toolkit calculates the Newman-Penrose scalar  $\psi_4$  (also called Weyl scalar 4)[22], which is linked to the GW strain  $h$  by the following relation, valid only at spatial infinity:

$$\psi_4 = \frac{\partial^2}{\partial t^2} (h_+ - i h_\times) \quad (39)$$

In order for equation(39) to be valid, the signal has to be extracted as furthest as possible from the source. The signal is then decomposed in spin-weighted spherical harmonics of spin  $-2$  by the thorn `Multipole`[23]

$$\psi_4(t', r, \theta, \phi) = \sum_{l=2}^{\infty} \sum_{m=-l}^{l=2} \psi_4^{lm}(t', r) {}_{-2}Y_{lm}(\theta, \phi)$$

The output given by the Einstein Toolkit is  $\psi_4^{lm}(t', r)$ . Since the dominant mode is  $l = m = 2$ , we consider  $\psi_4 = \psi_4^{l=2, m=2}$  and we extract the GW strain following a simplified procedure, which is similiar to the extraction method in [24]. A more advanced procedure can be found here [25]. Since  $\psi_4^{lm}(t', r)$  is extracted at a distance  $r$  from the source center, our data detect the signal at a time  $t'$ , which is different from the instant when the radiation was emitted. So, we subtract from the output time  $t'$  the distance from the source  $r$  in order to compute the gravitational radiation as if the signal would have been emitted at the coordinate origin.

We are interested in the behavior of the gravitational wave at a given time and distance  $(t, r) = (t' - r, r)$ , so we neglect the numerical factor  ${}_{-2}Y_{lm}(\theta, \phi)$  given by choosing an arbitrary angle  $(\theta, \phi)$  for the spin-weighted spherical harmonics. Thus, we integrate twice in time in order to get the complex-valued gravitational strain

$$\tilde{h}(t) = \int_0^t \int_0^{\hat{t}} \psi_4^{2,2}(t^*, r) dt^* d\hat{t}$$

where we used the trapezoidal rule for the numeric integration. The resulting quantity obtained with the procedure described above show a left-over drift in the GW. Performing a fit to a second order polynomial for both the real and the imaginary parts of  $\tilde{h}(t)$ , it is possible to eliminate as:

$$h_+(t) = \text{Re}\{\tilde{h}\} - (Q_0^R + Q_1^R t + Q_2^R t^2) \quad (40)$$

$$h_\times(t) = -\left[\text{Im}\{\tilde{h}\} - (Q_0^I + Q_1^I t + Q_2^I t^2)\right] \quad (41)$$

where the  $Q$  values are the coefficients of the fitted polynomials for the real  $Q^R$  and the imaginary  $Q^I$  parts of  $\tilde{h}(t)$ .

As we have seen in section(4.1) the gravitational radiation scales with the distance from the source as  $1/r$ . Therefore, in order to have a reasonable order of magnitude of the gravitational wave strain

$$h(t) = h_+ + i h_\times \quad (42)$$

where  $h_+$  and  $h_\times$  are taken from equations(40) and (41), we multiply  $h(t)$  by the distance at which it was measured and we divide it by a typical cosmological distance of binary sources  $r = 100 \text{ Mpc} \approx 3.1 \times 10^{19} \text{ km}$ .

| simulation name | par_b | par_m_plus | par_P_plus[1] |
|-----------------|-------|------------|---------------|
| BBH-b3          | 3     | 0.47656    | +0.13808      |
| BBH-b4          | 4     | 0.48243    | +0.11148      |
| BBH-b5          | 5     | 0.48595    | +0.095433     |
| BBH-b6          | 6     | 0.48830    | +0.084541     |
| BBH-b7          | 7     | 0.48997    | +0.076578     |
| BBH-b10         | 10    | 0.49299    | +0.061542     |

Table 1: The table shows the quasi-equilibrium initial conditions used in the `TwoPuncture` thorn. Since the two black holes have equal masses `par_m_plus=par_m_minus` and opposite momentum `par_P_plus[1]=-par_P_minus[1]`, we do not report in the table the obvious initial conditions of the second black hole.

## 5.2 Binary Black Hole

As we have done so far and following the Einstein Toolkit conventions, we set  $G = c = 1$ , and therefore we express time and space in units of solar masses  $M_\odot$ , i.e.  $1t[M_\odot] \approx 0.005\text{ms}$  and  $1x[M_\odot] \approx 1.5\text{km}$ .

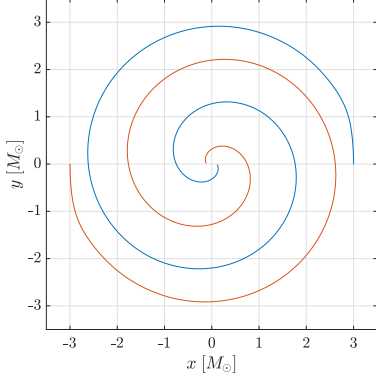
We simulate the evolution of equal-mass binary black holes using the parameter file included in the Einstein Toolkit [5] with different quasi-equilibrium initial conditions taken from [26]. The thorn `TwoPunctures` [27] is used to set up the initial data for the two black holes located on the x-axis with opposite linear momentum along the y-axis. Due to the symmetry of the problem, it is possible to reduce the computational cost by a factor of 2 by not evolving the domain with  $z < 0$ , and by another factor 2 evolving points with  $x > 0$  and populating the missing part by rotating the existing domain for 180 degrees along the z-axis [21]. An example of initial data set in the parameter file is

```
TwoPunctures::par_b = 3.0
TwoPunctures::par_m_plus = 0.47656
TwoPunctures::par_m_minus = 0.47656
TwoPunctures::par_P_plus [1] = +0.13808
TwoPunctures::par_P_minus[1] = -0.13808
```

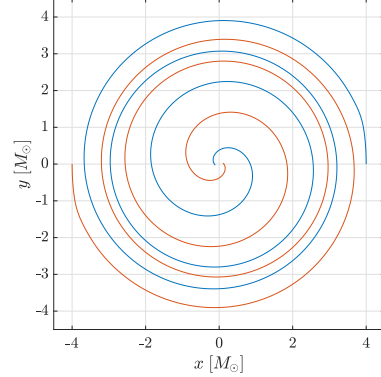
We call parameter  $b$  the parameter `par_b` which defines the initial distance of the two black holes at  $(x, y, z) = (\pm 3, 0, 0)$  from the origin of the axes. `par_m_plus` and `par_m_minus` set the "bare mass" parameter, and `par_P_plus[1]` and `par_P_minus[1]` set the Bowen-York linear momentum parameter. We let evolve the binary black hole using six different quasi-equilibrium initial conditions, Table(1). Each initial configuration is then evolved using the `ML_BSSN` (McLachlan BSSN) thorn [28, 29, 30].

The orbits of covered by the binaries black hole are shown in Figure(7). Due to the short initial distance from the origin, the BBHs with a low  $b$  merge after few revolutions, for instance BBH-b3 merges after 2 revolutions; BBH-b4 merges after 3.5 revolutions; BBH-b5 merges after 6 revolutions. Whereas the BBHs with an high parameter  $b$  have

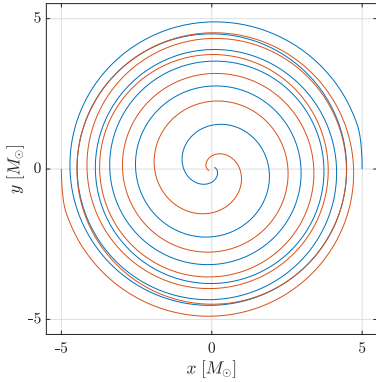
## Orbits of different configurations of BBH



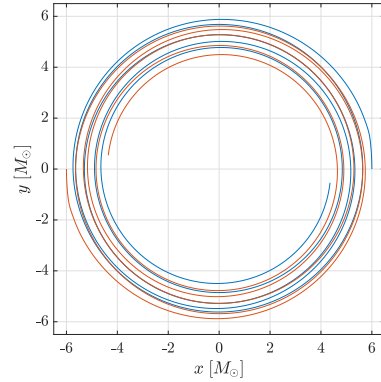
(a) Trajectory of the BBH with initial distance from the origin  $b = 3 M_{\odot}$ .



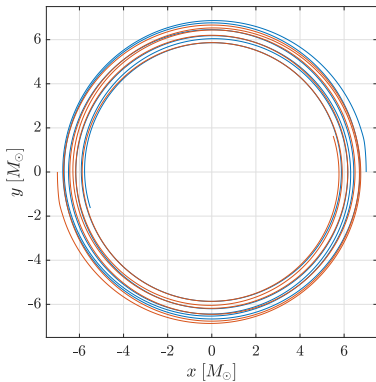
(b) Trajectory of the BBH with initial distance from the origin  $b = 4 M_{\odot}$ .



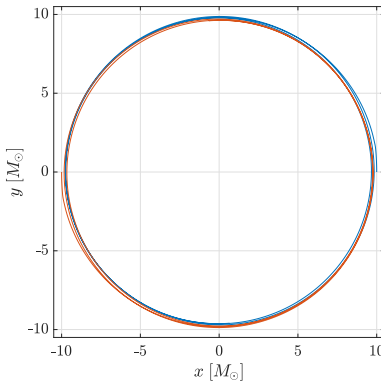
(c) Trajectory of the BBH with initial distance from the origin  $b = 5 M_{\odot}$ .



(d) Trajectory of the BBH with initial distance from the origin  $b = 6 M_{\odot}$ .



(e) Trajectory of the BBH with initial distance from the origin  $b = 7 M_{\odot}$ .



(f) Trajectory of the BBH with initial distance from the origin  $b = 10 M_{\odot}$ .

Figure 7: It is shown the evolution of the BBH using the quasi-equilibrium initial conditions of Table(1).

## Normalized radial evolution of the BBH

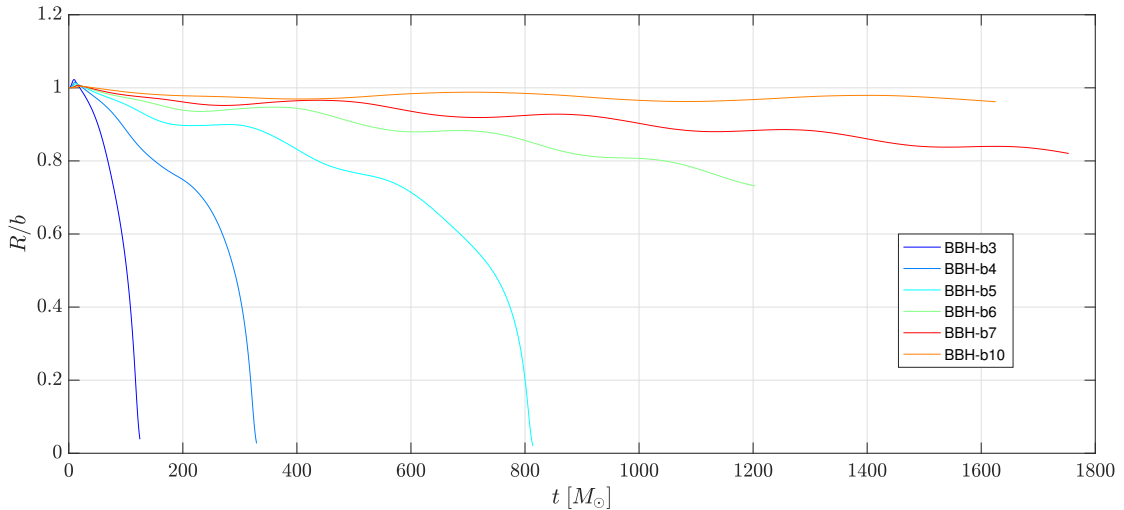


Figure 8: Time evolution of the distance  $R(t)$  between a black hole and the origin of the axes. The values are normalized to the initial separation from the origin  $b$ . The figure shows oscillation modes especially for BBHs with high  $b$ .

orbits close to each other, such that they form a ring shape.

Notice that as the  $b$  increases, the two black holes have orbits that drift apart from the coil-shaped path of Figure(7a). This behavior can be better understood analyzing the distance of one of the black hole from the origin as a function of time. For this reason, we plot in Figure(8) the normalized radial distance

$$R(t)/b = \frac{\sqrt{x^2(t) + y^2(t)}}{b}$$

which shows oscillations of the time-evolution of the radius  $R(t)$  for high values of  $b$ . Notice also that the time of the merger increases non linearly as we increases  $b$  in the quasi-equilibrium configurations.

We now study the gravitational radiation emitted by the binary sources of Table(1). The gravitational wave is extracted following to the procedure described in section(5.1). The gravitational signals are shown in Figure(9), (10), (11), (12), (13) and (14) and the time units are in ms. In the time interval  $t \in (0, 0.1)$ ms the  $\psi_4$  of all simulations shows an irregular perturbation. In [5] it is pointed out that there is a numerical noise that could be reduced using a more refined simulations. However, the simulations are enough accurate for our purpose after that time interval.

## Gravitational Wave emitted by BBH-b3

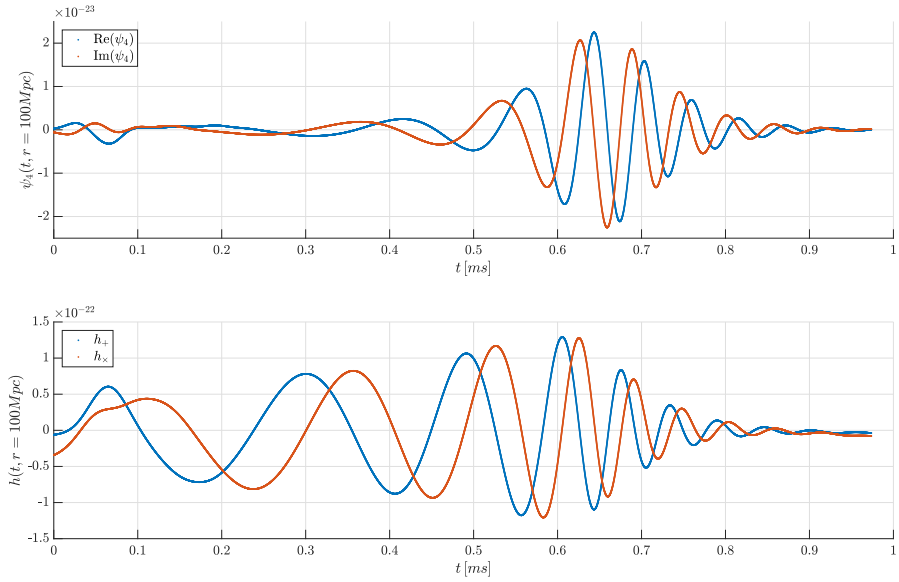


Figure 9: The first and the second panels show, respectively the gravitational signal  $\psi_4 = \psi_4^{2,2}$  and the gravitational strain produced by the BBH-b3.

## Gravitational waves emitted by BBH-b4

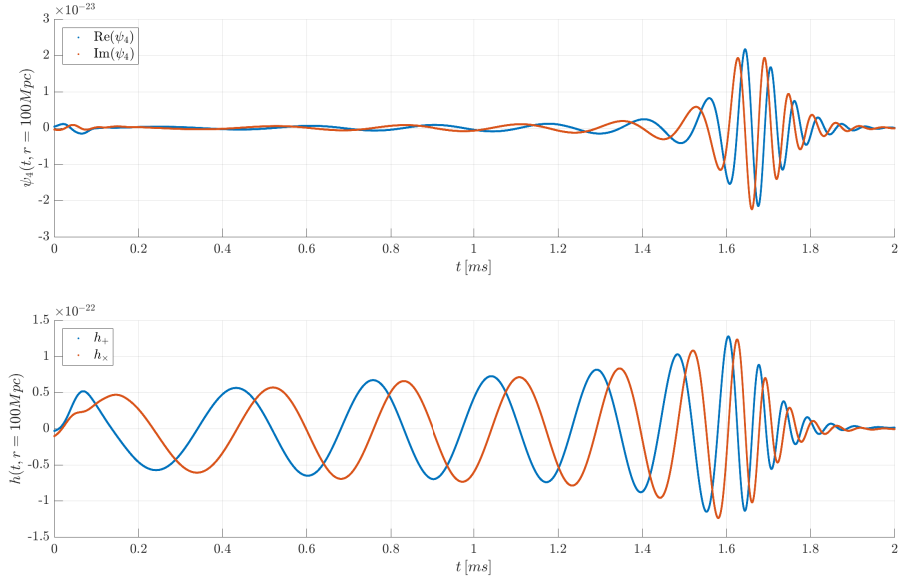


Figure 10: The first and the second panels show, respectively the gravitational signal  $\psi_4 = \psi_4^{2,2}$  and the gravitational strain produced by the BBH-b4.

## Gravitational waves emitted by BBH-b5

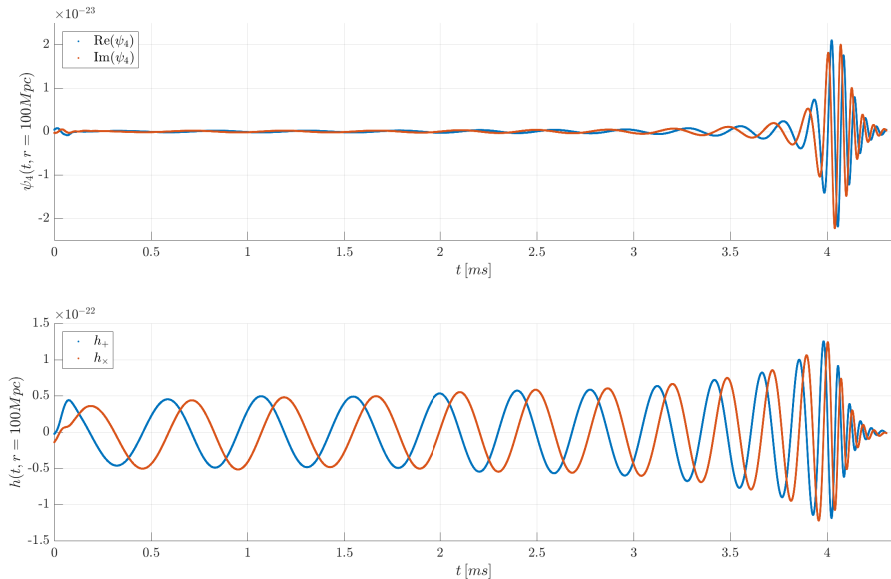


Figure 11: The first and the second panels show, respectively the gravitational signal  $\psi_4 = \psi_4^{2,2}$  and the gravitational strain produced by the BBH-b5.

The GW radiated by the binary black hole with parameter  $b = 3$ , in Figure(9), has a short duration with respect to the others due to the intial conditions. In fact, due to the strong interaction between the two bodies, the black holes merge quickly after  $125 M_\odot \approx 0.616$  ms from Figure(8). The radius of the orbit decreases rapidly and the inspiralling phase lasts only 0.6ms and, as a consequence the waveform is a sinusoid with a noticeable varying frequency. After 6.1ms the gravitational wave aplitude starts decreasing and oscillating around zero as expected in the ring-down phase, in which the black holes are already merged.

The gravitational radiations emitted of BBH-b4 and BBH-b5 are pretty similiar, they both show the typical phase of insipralling that can be approximated with a sinusoid analogue to the quadrupole formula. Since the BBH-b5 has a initial configuration with further initial separation than BBH-b4, the signal of BBH-b5 lasts longer 4.5ms than the GW radiaitaiion of BBH-b4 lasting 2ms.

The gravitational strains  $h$  of BBH-b3, BBH-b4 and BBH-b5 have similiar amplitudes, the strain increases its vale from  $\approx 0.5 \times 10^{-22}$  up to  $\approx 1.5 \times 10^{-22}$  during the inspiralling, and the ring-doww phase lasts approximately 0.5 ms.

The gravitational signal  $\psi_4$  radiated by the BBH-b6 source has big initial noise and it is affected by perturbations between (1, 1.5)ms. These perturbations are washed out with the gravitational wave extraction method, indeed, Figure(12) shows a smooth gravitational strain  $h$ . In a time interval of 5ms the amplitudes of the two polarizations  $h_+$  and  $h_x$  of BBH-b6 vary, respectively, from  $3.9 \times 10^{-23}$  to  $5 \times 10^{-23}$ , and from  $3 \times 10^{-23}$  up to

$$4.5 \times 10^{-23}.$$

As expected, by increasing the parameter  $b$ , the gravitational strain decreases in intensity in the first part of the black hole evolution of BBH-b7 and BBH-b10. The  $\psi_4$  signals produced by BBH-b7 and BBH-b10 manifest a new feature in the gravitational strain  $h$ . It is evident from Figures (14) and (13) that the two polarization  $h_+$  and  $h_\times$  have another oscillation mode with larger period. We guess that those oscillations are related to the oscillations in the radial evolution.

We give two possible causes of such behavior. The strong curvature due to the two black holes might generate gravitational perturbations propagating inwards, and therefore, influencing each others trajectories. Or, another cause could be that the results of the simulations are affected by a numerical noise. However, a more accurate analysis is needed to confirm one of the two hypothesis or none of them.

Despite the fact that the quadrupole formula cannot be used for black holes, the inspiralling phase of BBH-b6, BBH-b7, BBH-b10 could be well approximated by the quadrupole formula as we can see from the waveform.

### Gravitational waves emitted by BBH-b6

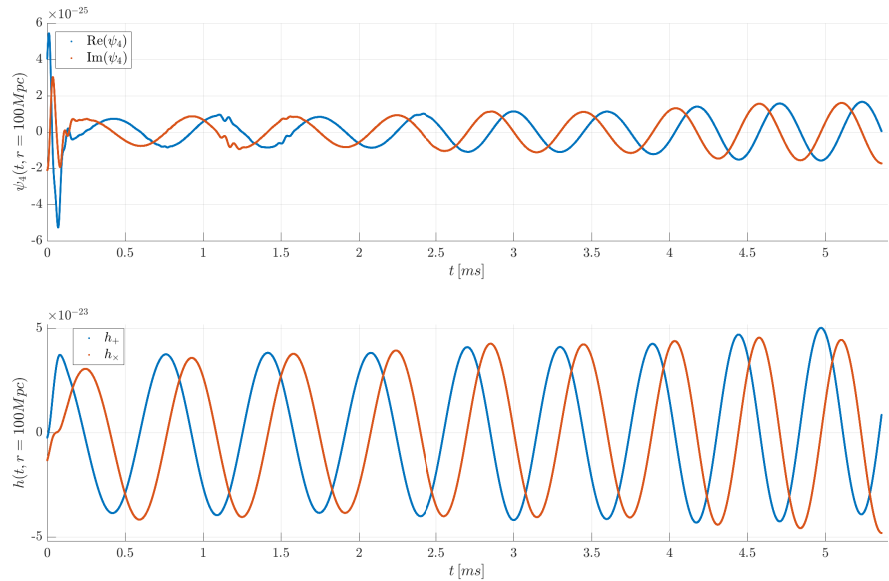


Figure 12: The first and the second panels show, respectively the gravitational signal  $\psi_4 = \psi_4^{2,2}$  and the gravitational strain produced by the BBH-b6.

## Gravitational waves emitted by BBH-b7

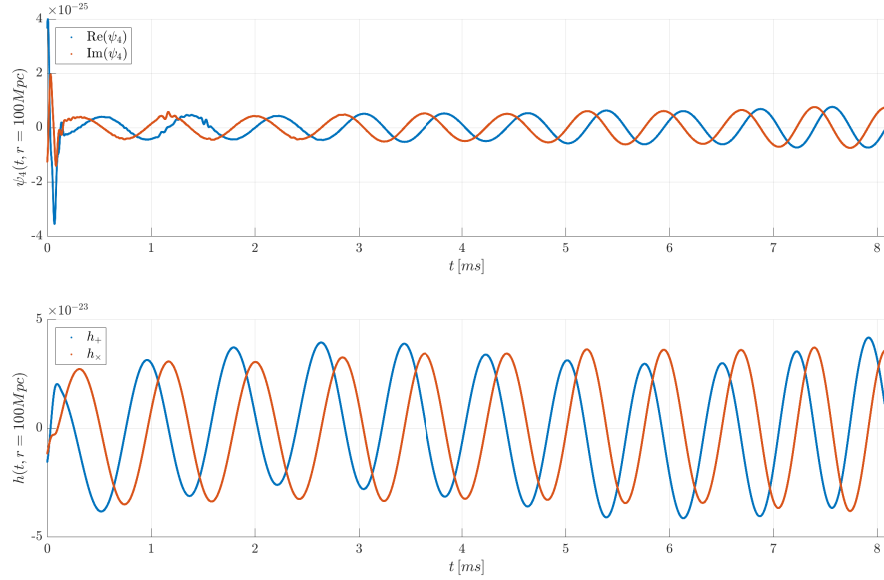


Figure 13: The first and the second panels show, respectively the gravitational signal  $\psi_4 = \psi_4^{2,2}$  and the gravitational strain produced by the BBH-b7.

## Gravitational waves emitted by BBH-b10

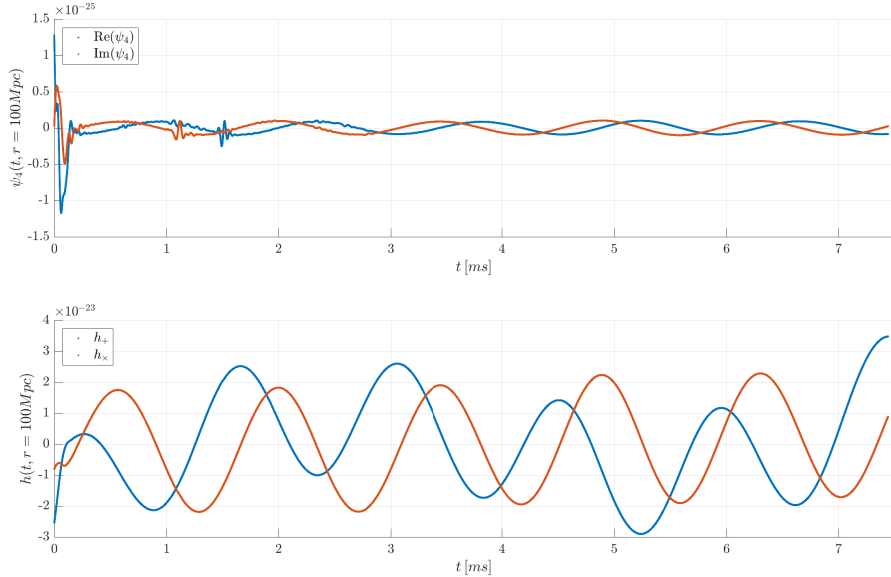


Figure 14: The first and the second panels show, respectively the gravitational signal  $\psi_4 = \psi_4^{2,2}$  and the gravitational strain produced by the BBH-b10.

An important result obtained through the quadrupole formula applied to a binary source was that the frequency of the gravitational wave is twice the orbital frequency of rotating bodies. Using the Fourier transform of the gravitational strain and the angular frequency data of the black holes we can test this hypothesis.

We plot in Figures (15) and (16), on the left side, the normalized absolute value of the Fourier transform of the gravitational wave strain:

$$|\mathcal{F}[h(t, r = 100 \text{ Mpc})]| = \left| \frac{\int e^{i\omega t} h(t, r = 100 \text{ Mpc}) dt}{\max [\int e^{i\omega t} h(t, r = 100 \text{ Mpc}) dt]} \right|$$

and on the right side the orbital angular frequency of the BBHs:

$$\omega = \frac{x v_y - y v_x}{x^2 + y^2}$$

where  $x$  and  $y$  are the coordinates of one of the BH, whereas  $v_x$  and  $v_y$  are the velocities along respectively the x and y axis.

Figures (15b), (15d) and (15f) show that the orbital angular velocity increases more rapidly for higher values of  $b$  during the last stage of the simulation. This aspect cannot be seen from Figures (16b), (16d) and (16f), because the simulations do not last enough for the black holes to merge. However, the orbital frequency of BBH-b6, BBH-b7, BBH-b10 manifest the typical oscillations that we have also noticed in the previous discussions. The Fourier transform allows us to study the range of angular frequencies of the GWs. In Figures (15a), (15c) and (15e) it is evident a peak on an angular frequency that is approximately twice the mean value of the orbital angular frequencies of the rotating black in Figures (15b), (15d) and (15f). Notice that the peak is more narrow for higher values of  $b$ , since the initial sinusoidal behavior of the gravitational wave is more evident and longer for simulations with high  $b$ .

The BBH-b6, BBH-b7 and BBH-b10 depict, as well, the typical peak at twice the orbital angular frequency. We confirm that the gravitational wave strain of a binary black holes source has an angular frequency at twice the orbital angular frequency of the rotating bodies.

Although the peaks are particularly sharp, each Figure (16a), (16c) and (16e) manifest a smaller peak at lower frequencies, which has an increasing intensity with the increasing parameter  $b$ . Such phenomenon could be due to the oscillations of the BBHs that we discussed previously.

## Fourier transforms of the gravitational strain $\mathcal{F}[h](\omega)$ and orbital angular velocities $\omega$ of BBH-b3, BBH-b4 and BBH-b5

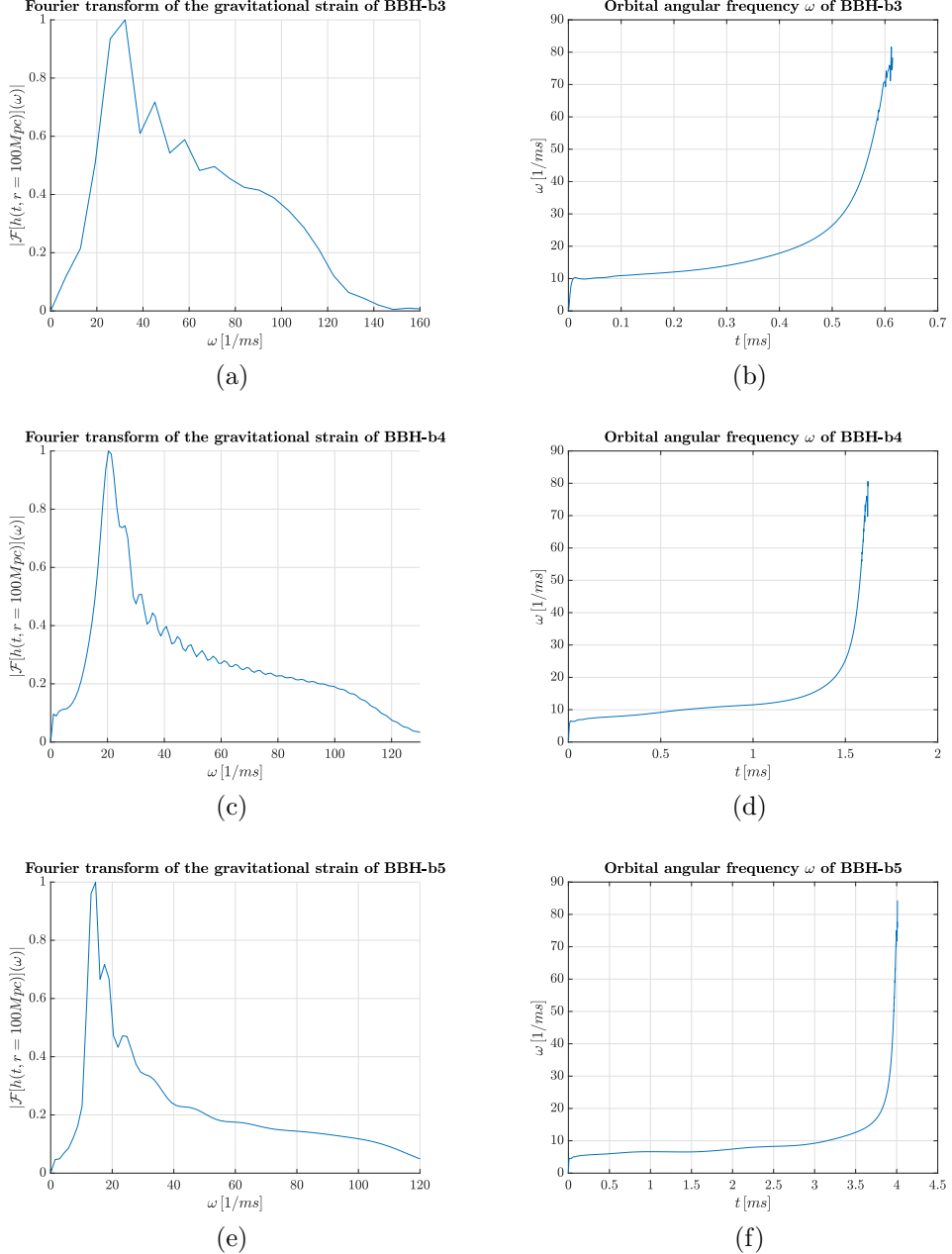


Figure 15: The Figures shows the absolute value of normalized Fourier transform of  $h(t)$  and the orbital angular velocities  $\omega$  of the different binaries. The Fourier transform has a peak approximately on the mean value of the orbital angular velocity.

## Fourier transforms of the gravitational strain $\mathcal{F}[h](\omega)$ and orbital angular velocities $\omega$ of the BBH-b6, BBH-b7 and BBH-b10

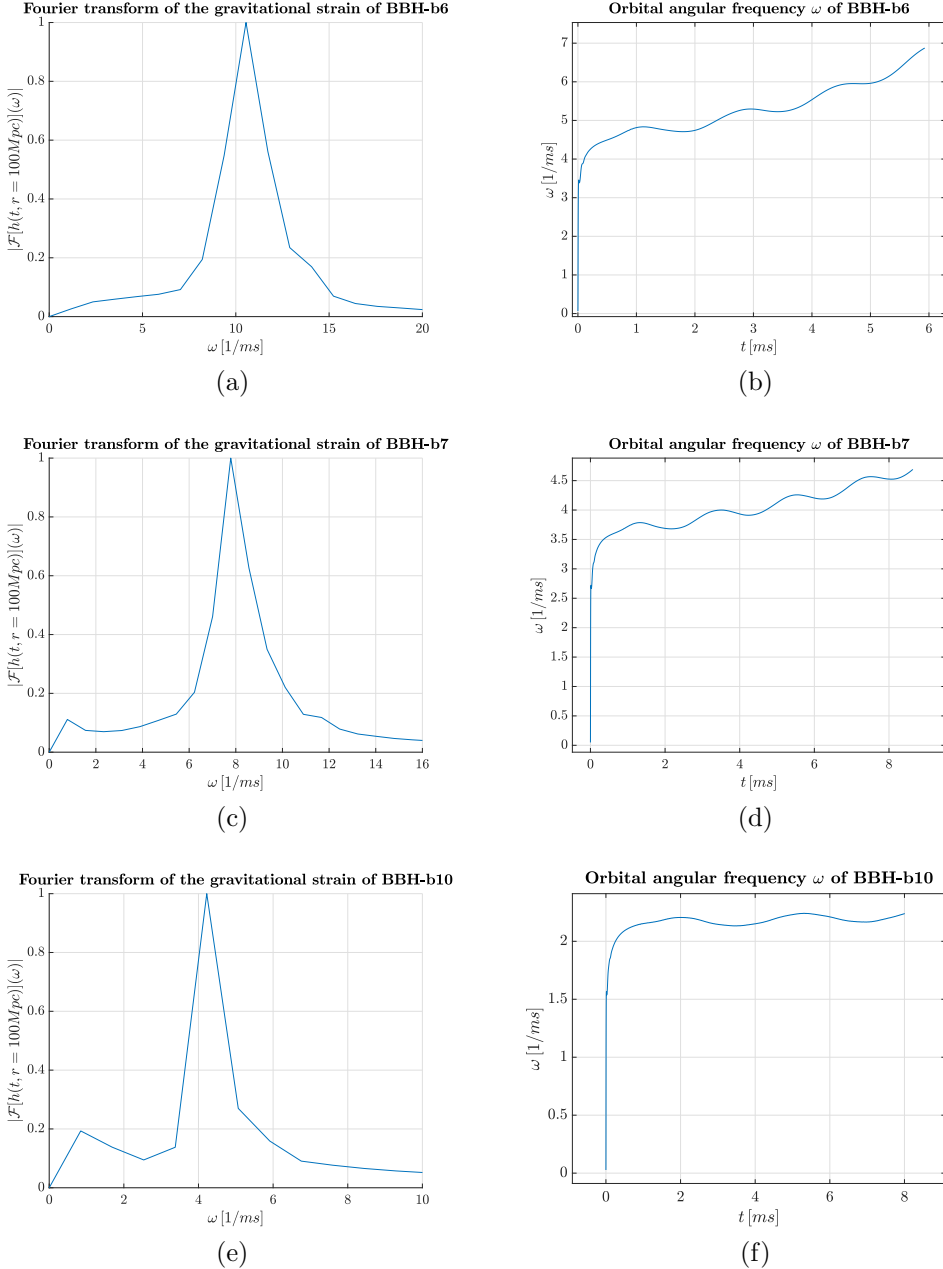


Figure 16: The Figures shows the absolute value of normalized Fourier transform of  $h(t)$  and the angular velocities of the different binaries. The Fourier transform has a peak approximately on the mean value of the orbital angular velocity. There is also another smaller peak at lower values of  $\omega$  in Figure(16e). The orbital angular frequency shows an oscillation that is linked to the oscillation of the radius in Figure(8).

### 5.3 Binary Neutron Star

We now study the evolution of a binary neutron star (BNS) made of two equal-mass objects rotating with an quasi-equilibrium initial conditions obtained using the software `Lorene` [31]. The total ADM mass of the system is  $M_{\text{ADM}} = 3.251 M_{\odot}$ . Since the two neutron stars are placed at symmetric initial conditions with respect to the z axis the computational cost can be reduced, as in the BBH simulations. The hydrodynamics evolution of the neutron stars is achieved using the ideal fluid approximation and the thorn `GRHydro` [32]. The link between pressure  $P$  and density  $\rho$  is provided by the following equation of state (EOS)

$$P = K \rho^{\Gamma}$$

where  $K$  is the polytropic constant and  $\Gamma$  is the adiabatic index.

The initial separation between the two neutron stars is set to be  $45 \text{ km} \approx 30.47 M_{\odot}$ , whereas we set  $K = 123.6$  and  $\Gamma = 2$ .

#### Gravitational wave and orbital radius of the BNS

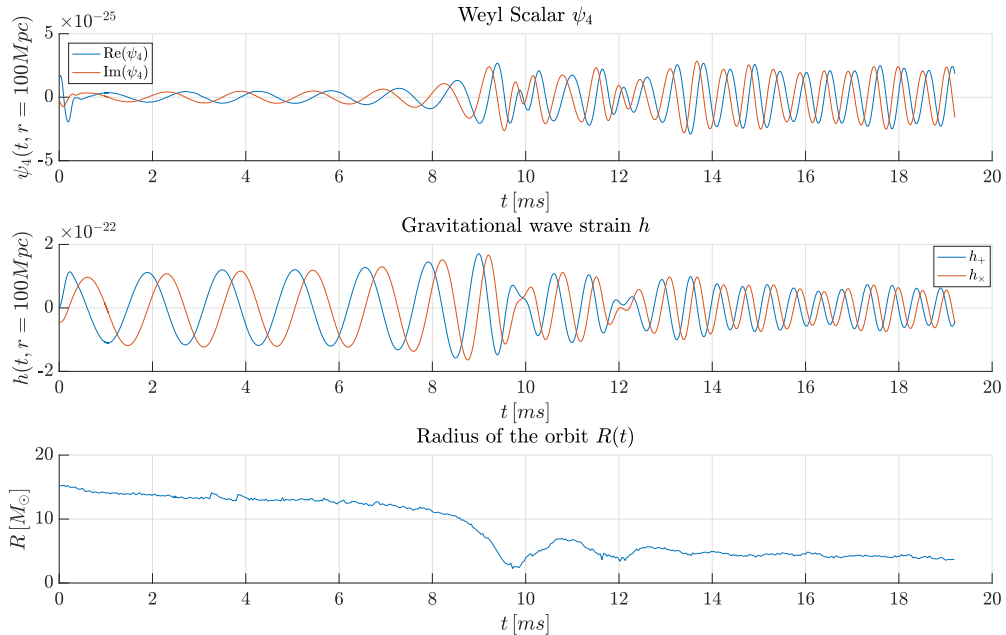


Figure 17: The first and the second panels show, respectively the gravitational signal  $\psi_4 = \psi_4^{2,2}$  produced by the BNS, whereas the third pane shows the orbital radius obtained defined as the highest value of the density. Notice the bouncing behavior after  $t \approx 9\text{ms}$ , when the stars start bouncing and the gravitational wave amplitude decreases slowly.

The gravitational wave strain  $h$  is extracted following the procedure in section(5.1),

whereas the orbital radius  $R$  is obtained calculating the highest value of density  $\rho$  at each time step.

The gravitational wave and the orbital radius are shown in Figure(17). During the inspiralling phase  $t \in (0, 8.5)$  ms, the gravitational wave is similar to that one of the binary black holes, indeed, BNS and BBH both show a sinusoid with an increasing frequency. However, when the strain reaches the highest value approximately at  $t \approx 9$  ms, the signal does not drop off as rapidly as for the black holes, but it rebounds while slowly decreasing. The orbital radius  $R$  shows an analogue behavior, in fact, it reaches the lowest value right at  $t \approx 9.9$  ms and then it bounces around  $R \approx 4 M_{\odot}$ .

The reason of such behavior relies on the differences between a black hole and a neutron star. However, since we could not continue simulations for a longer time, we cannot describe the features of the waveform in detail, but we speculate on the expected outcome and discuss the significance of the waveforms from the observational point of view. Due to the nature of black holes, the ring-down phase is short because when the events of horizon are enough close, the black holes merge into single black hole which shrinks quickly. So, the gravitational waveform amplitude of the BHs damps rapidly after the merger.

In general, massive objects such neutron stars could collapse under their own weight forming a black hole. The compactness of the neutron stars is a crucial parameter which determines if the a black hole is formed after the merger [33, 34]. If the neutron stars merge into a black hole, the gravitational wave strain manifests a ring-down phase similar to that one of the binary black holes. In our case, we speculate that the binary neutron stars do not form a black hole, because they are not enough compact and they transfer matter between themselves and outwards.

In order to analyze the matter distribution during the simulation, let us study the rest mass density during the time evolution of the BNS.

A video of the rest mass density evolution can be downloaded at [https://github.com/lorenzsp/thesis/blob/master/binary\\_ns\\_video/bns.mp4](https://github.com/lorenzsp/thesis/blob/master/binary_ns_video/bns.mp4)

In Figure (18) it is shown the initial stage of the BNS evolution. From Figure(18a) it is possible to notice how the gravitational attraction between the two objects slightly reshapes their surfaces. After  $t = 3.83$  ms =  $777.6 M_{\odot}$  the stars start transferring matter between themselves, meanwhile a stream of matter is being ejected (Figure(18c)).

When the gravitational strain reaches the highest amplitude  $\approx 9$  ms, the neutron stars have a prolate shape (Figure(18d)). Instead of merging, the neutron stars bounce off again and again during the final stage of the evolution Figure(19). Such behavior and the high rotational velocity lead the system to eject a big amount of matter, during the ring-down phase (Figures(19a) and (19b)). The matter, that does not overcome the "centrifugal force", is thrown away in a spiralling shape. The bounce of the neutron stars is associated to the oscillation of the gravitational wave amplitude in Figure(17).

## Initial stage of the rest mass density evolution

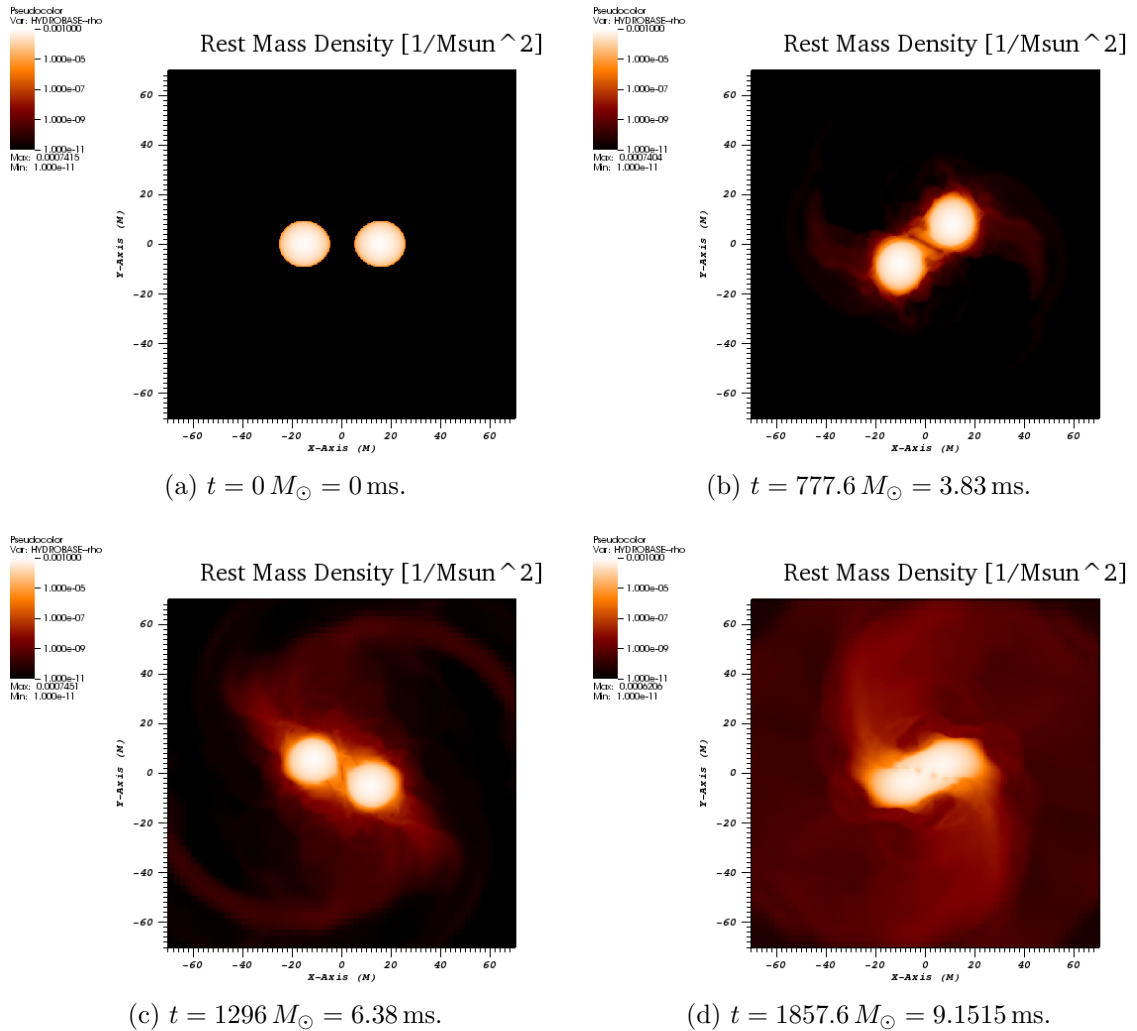


Figure 18: The rest mass density of the binary neutron star evolves from an initial separation of  $30.47 M_\odot$ . We can notice that already from  $t = 777.6 M_\odot$  the matter starts to be ejected and exchanged between the two stars.

## Final stage of the rest mass density evolution

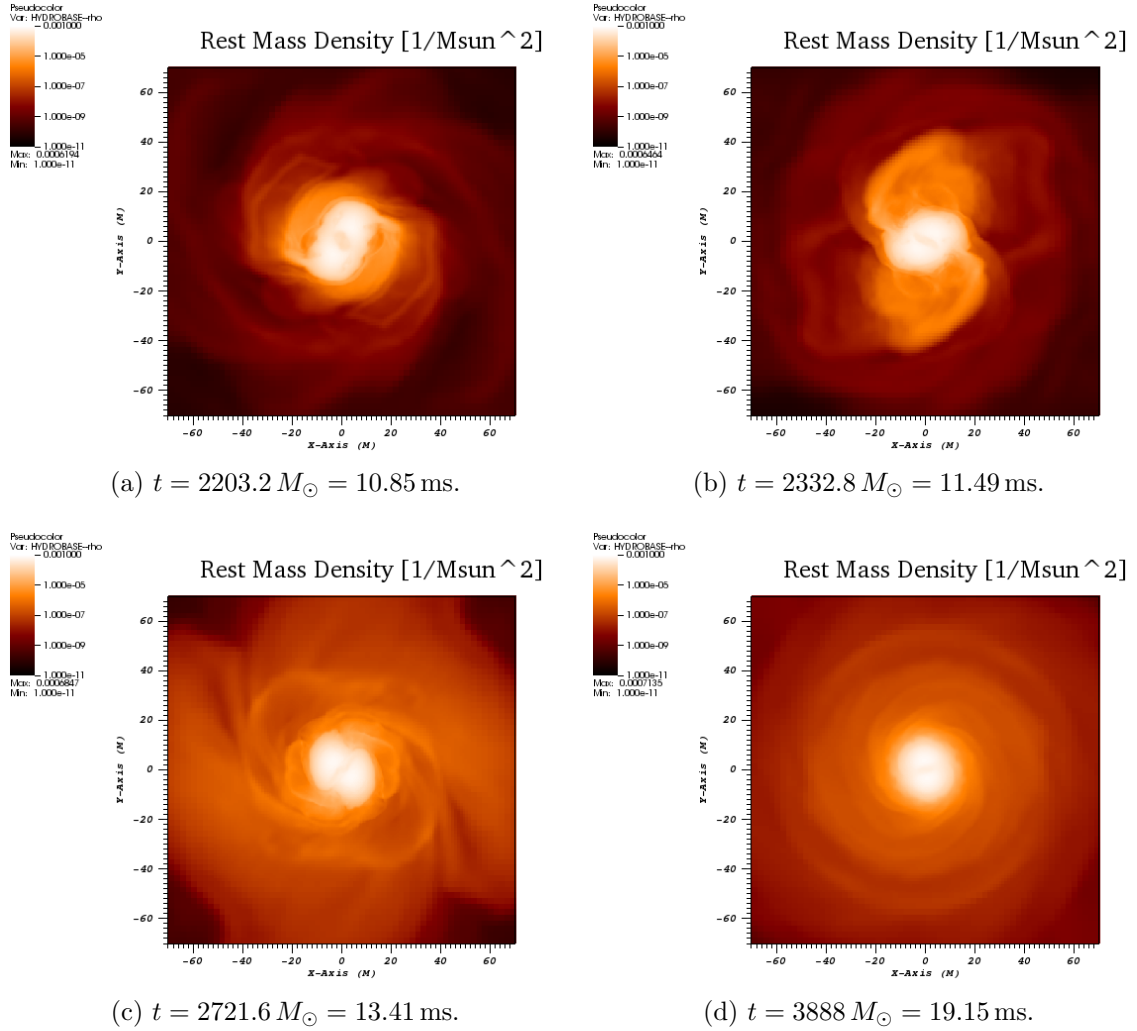


Figure 19: The rest mass density evolution in the final stage is dominated by an ejection of matter. The neutron stars' cores bounce back and forth and releases matter in an inspiral shape, this feature of the evolution is imprinted in the gravitational wave in Figure(17).

## Fourier transforms of the gravitational strain $\mathcal{F}[h](\omega)$ and orbital angular velocities $\omega$ of BNS

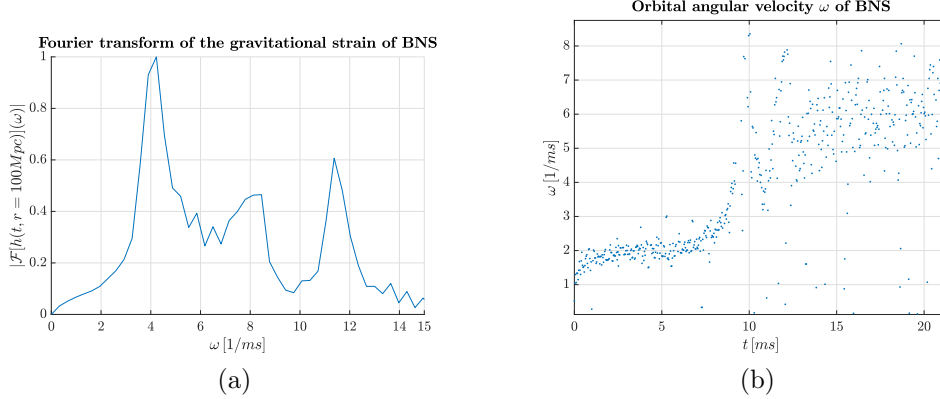


Figure 20: The Fourier transform of the gravitational strain  $|\mathcal{F}[h]|$  shows a broad distribution of angular frequencies, however the two highest peaks are at  $\omega = 4.3\text{ms}^{-1}$  and at  $\omega = 5.5\text{ms}^{-1}$ . On the right side the orbital angular momentum of the binary system is stable around  $2\text{ms}^{-1}$  before the merger. After 10ms the orbital angular momentum is in a range  $(4.5, 7)\text{ms}^{-1}$ .

We study the angular frequency spectrum of the gravitational waves from Figure(20). Nevertheless, the orbital angular frequency is characterized by a lot of noise<sup>2</sup>, it is possible anyway to see that the  $\omega$  has a value approximately  $2\text{ ms}^{-1}$  before the merger, and a value approximately  $6\text{ ms}^{-1}$  after the merging. As expected from the quadrupole formula, the gravitational wave has an angular frequency that is twice the orbital angular frequency for that mentioned values.

---

<sup>2</sup>the values of  $\omega$  are particularly spread out because of the low sampling frequency and problems in the acquisition of data. It is possible to better appreciate this reasons analyzing the data given at <https://github.com/lorenzsp/thesis/tree/master/gw>

## 6 Conclusions

Using the weak field linearized equation, the Einstein's field equation in vacuum reduces to a tensorial form of the wave equation (11), which tells us that the metric perturbation behaves as a wave and it travels at the speed of light. So, the metric perturbation is nothing but a propagating warpage of spacetime, that we call gravitational wave.

Using the transverse traceless gauge, we saw that the polarization states of the gravitational radiation are only two:  $h_+$  and  $h_\times$ . The two polarization modes are directly related to the way they stretch and squeeze spacetime and, therefore, they can change the proper distance between free falling particles according in the shape of + or  $\times$ . Such effect can be exploited to detect gravitational waves using interferometers.

We analyzed the nature of gravitational wave and we found out that it has quadrupolar nature and the GW amplitude scales as  $1/r$ . We derived the quadrupole formula stressing the importance of the approximations and we applied it to a slowly moving binary system. The main result of such example told us that the gravitational wave radiation has a frequency that is twice the orbital angular frequency.

Subsequently we studied the simulations of two compact binaries, and through a Fourier analysis we confirmed that the angular frequency of the gravitational waves of BBH and BNS is twice the orbital angular frequency.

The orbital angular frequency is almost constant for the first part of the inspiralling phase, and therefore, in this time range it is possible to recognize a sinusoidal behavior of the gravitational wave similar to the quadrupole formula approximation. However, the binary system loses energy in the emission of gravitational waves and, therefore, the radius of the binary system decreases. As the radius decreases, the orbital angular frequency increases, and therefore, the angular frequency of the gravitational wave does as well. During the evolution the amplitude of the GW increases until it reaches the maximum value before the merger. Both BBH and BNS show similar gravitational signals during the inspiralling phase.

For a binary black hole, the gravitational wave signal is damped after the merger, whereas for the considered binary neutron star, the radiation amplitude slowly decreases. Furthermore, the bouncing in the gravitational wave amplitude of the BNS denotes that the cores are bouncing off each other.

In addition, we tested successfully the codes provided by the Einstein Toolkit [7], and we also tested the quasi-equilibrium initial conditions of [26].

Further researches and more accurate simulations should be done in order to precisely explain the oscillations mode of the orbital angular frequency and of the gravitational strain of BBH-b6, BBH-b7, BBH-b10.

We have analyzed only few of the many features that can be obtained from the gravitational wave signals. In fact, by combining the powerful computational knowledge of numerical relativity with the new "eyes" given by the gravitational wave detectors, it is possible to study thoroughly fascinating astrophysical processes involving black holes mergers and neutron star gamma ray bursts.

## Acknowledgements

I wish to acknowledge the help received from some people and organizations during the developing of this project.

First and foremost, i must thank my supervisor, prof. Bruno Giacomazzo, who introduced me to the fascinating world of numerical relativity through the Einstein Toolkit. I would also like to acknowledge the computational physics group at the University of Oslo, for providing me the access to the cluster "Smaug". Without the compuational power of "Smaug", I would have not run the numerical simulations shown in this work. I would also like to thank Giovanni Pederiva, who constantly taught me many crucial numerical concepts.

Finally, I must express my very profound gratitude to my family, my girlfriend and my friends for providing me with unfailing support and continuous encouragement. This accomplishment would not have been possible without them.

Thank you.

Lorenzo Speri

## References

- [1] J. M. Weisberg and J. H. Taylor. “Relativistic Binary Pulsar B1913+16: Thirty Years of Observations and Analysis”. In: *arXiv:astro-ph/0407149* (July 7, 2004). arXiv: [astro-ph/0407149](https://arxiv.org/abs/astro-ph/0407149). URL: <http://arxiv.org/abs/astro-ph/0407149> (visited on 04/07/2018).
- [2] Joel M. Weisberg, David J. Nice, and Joseph H. Taylor. “Timing Measurements of the Relativistic Binary Pulsar PSR B1913+16”. In: *The Astrophysical Journal* 722.2 (Oct. 20, 2010), pp. 1030–1034. ISSN: 0004-637X, 1538-4357. DOI: [10.1088/0004-637X/722/2/1030](https://doi.org/10.1088/0004-637X/722/2/1030). arXiv: [1011.0718](https://arxiv.org/abs/1011.0718). URL: <http://arxiv.org/abs/1011.0718> (visited on 04/07/2018).
- [3] B.P. Abbott et al. “Observation of Gravitational Waves from a Binary Black Hole Merger”. In: *Physical Review Letters* 116.6 (Feb. 11, 2016). ISSN: 0031-9007, 1079-7114. DOI: [10.1103/PhysRevLett.116.061102](https://doi.org/10.1103/PhysRevLett.116.061102). URL: <https://link.aps.org/doi/10.1103/PhysRevLett.116.061102> (visited on 07/04/2018).
- [4] B.P. Abbott et al. “GW170817: Observation of Gravitational Waves from a Binary Neutron Star Inspiral”. In: *Physical Review Letters* 119.16 (Oct. 16, 2017). ISSN: 0031-9007, 1079-7114. DOI: [10.1103/PhysRevLett.119.161101](https://doi.org/10.1103/PhysRevLett.119.161101). URL: <https://link.aps.org/doi/10.1103/PhysRevLett.119.161101> (visited on 07/04/2018).
- [5] Frank Löffler et al. “The Einstein Toolkit: A Community Computational Infrastructure for Relativistic Astrophysics”. In: *Classical and Quantum Gravity* 29.11 (June 7, 2012), p. 115001. ISSN: 0264-9381, 1361-6382. DOI: [10.1088/0264-9381/29/11/115001](https://doi.org/10.1088/0264-9381/29/11/115001). arXiv: [1111.3344](https://arxiv.org/abs/1111.3344). URL: <http://arxiv.org/abs/1111.3344> (visited on 05/03/2018).
- [6] codata\_blog. *CODATA Recommended Values of the Fundamental Physical Constants: 2014 — CODATA Blog*. URL: <https://codata.org/blog/2015/08/04/codata-recommended-values-of-the-fundamental-physical-constants-2014/> (visited on 04/14/2018).
- [7] Einstein Toolkit: Open software for relativistic astrophysics. URL: <http://einstein toolkit.org/>.
- [8] Galina Weinstein. “Einstein’s Discovery of Gravitational Waves 1916-1918”. In: *arXiv:1602.04040 [physics]* (Feb. 2016). arXiv: [1602.04040 \[physics\]](https://arxiv.org/abs/1602.04040).
- [9] Sean Carroll. *Spacetime and Geometry: An Introduction to General Relativity*. San Francisco: Pearson, Sept. 28, 2003. 513 pp. ISBN: 978-0-8053-8732-2.
- [10] Eanna E. Flanagan and Scott A. Hughes. “The basics of gravitational wave theory”. In: *New Journal of Physics* 7 (Sept. 29, 2005), pp. 204–204. ISSN: 1367-2630. DOI: [10.1088/1367-2630/7/1/204](https://doi.org/10.1088/1367-2630/7/1/204). arXiv: [gr-qc/0501041](https://arxiv.org/abs/gr-qc/0501041). URL: <http://arxiv.org/abs/gr-qc/0501041> (visited on 04/17/2018).

- [11] Nigel T. Bishop and Luciano Rezzolla. “Extraction of Gravitational Waves in Numerical Relativity”. In: *Living Reviews in Relativity* 19.1 (Dec. 2016). ISSN: 2367-3613, 1433-8351. DOI: [10.1007/s41114-016-0001-9](https://doi.org/10.1007/s41114-016-0001-9). arXiv: [1606.02532](https://arxiv.org/abs/1606.02532). URL: <http://arxiv.org/abs/1606.02532> (visited on 04/28/2018).
- [12] Martin Hendry. *An Introduction to General Relativity, Gravitational Waves and Detection Principles*. URL: [http://www.astro.gla.ac.uk/~martin/teaching/gravitational-wave-detection/supa\\_gwd\\_mah.pdf](http://www.astro.gla.ac.uk/~martin/teaching/gravitational-wave-detection/supa_gwd_mah.pdf) (visited on 06/30/2018).
- [13] Kip S. Thorne. “Gravitational Waves”. In: *arXiv:gr-qc/9506086* (June 30, 1995). arXiv: [gr-qc / 9506086](https://arxiv.org/abs/gr-qc/9506086). URL: <http://arxiv.org/abs/gr-qc/9506086> (visited on 06/23/2018).
- [14] “LIGO: The Laser Interferometer Gravitational-Wave Observatory Author(s): Alex Abramovici, William E. Althouse, Ronald W. P. Drever, Yekta Gürsel, Seiji Kawamura, Frederick J. Raab, David Shoemaker, Lisa Sievers, Robert E. Spero, Kip S. Thorne, Rochus E. Vogt, Rainer Weiss, Stanley E. Whitcomb, Michael E. Zucker”. In: *Science, New Series* 256.5055, (1992), pp. 325–333.
- [15] C J Moore, R H Cole, and C P L Berry. “Gravitational-Wave Sensitivity Curves”. In: *Classical and Quantum Gravity* 32.1 (Jan. 2015), p. 015014. ISSN: 0264-9381, 1361-6382. DOI: [10.1088/0264-9381/32/1/015014](https://doi.org/10.1088/0264-9381/32/1/015014).
- [16] M. Leclerc. “Geodesic Deviation and Gravitational Waves”. In: *arXiv:gr-qc/0605033* (May 2006). arXiv: [gr-qc/0605033](https://arxiv.org/abs/gr-qc/0605033).
- [17] Bernard F. Schutz. *A first course in general relativity*. Cambridge [Cambridgeshire]; New York: Cambridge University Press, 1985. 376 pp. ISBN: 978-0-521-25770-1 978-0-521-27703-7.
- [18] Valeria Ferrari. “THE QUADRUPOLE FORMALISM APPLIED TO BINARY SYSTEMS”. In: () .
- [19] Collaborative Effort. *Einstein Toolkit for Relativistic Astrophysics*. Astrophysics Source Code Library. Feb. 2011. eprint: [ascl:1102.014](https://ascl.net/1102.014).
- [20] *Cactus Code*. URL: <http://cactuscode.org/> (visited on 06/30/2018).
- [21] Miguel Zilhão and Frank Löffler. “An Introduction to the Einstein Toolkit”. In: *International Journal of Modern Physics A* 28.22n23 (Sept. 2013), p. 1340014. ISSN: 0217-751X, 1793-656X. DOI: [10.1142/S0217751X13400149](https://doi.org/10.1142/S0217751X13400149). arXiv: [1305.5299](https://arxiv.org/abs/1305.5299).
- [22] Ezra Newman and Roger Penrose. “An Approach to Gravitational Radiation by a Method of Spin Coefficients”. In: *Journal of Mathematical Physics* 3 (May 1, 1962). ISSN: 0022-2488. DOI: [10.1063/1.1724257](https://doi.org/10.1063/1.1724257). URL: <https://aip.scitation.org/doi/10.1063/1.1724257> (visited on 07/01/2018).
- [23] Kip S. Thorne. “Multipole expansions of gravitational radiation”. In: *Rev. Mod. Phys.* 52 (Apr. 1, 1980). DOI: [10.1103/RevModPhys.52.299](https://doi.org/10.1103/RevModPhys.52.299). URL: <https://link.aps.org/doi/10.1103/RevModPhys.52.299> (visited on 07/01/2018).

- [24] Roberto De Pietri et al. “Modeling Equal and Unequal Mass Binary Neutron Star Mergers Using Public Codes”. In: *Physical Review D* 93.6 (Mar. 21, 2016). ISSN: 2470-0010, 2470-0029. DOI: [10.1103/PhysRevD.93.064047](https://doi.org/10.1103/PhysRevD.93.064047). arXiv: [1509.08804](https://arxiv.org/abs/1509.08804). URL: <http://arxiv.org/abs/1509.08804> (visited on 03/14/2018).
- [25] Francesco Maione et al. “Spectral analysis of gravitational waves from binary neutron star merger remnants”. In: *Physical Review D* 96.6 (Sept. 19, 2017). ISSN: 2470-0010, 2470-0029. DOI: [10.1103/PhysRevD.96.063011](https://doi.org/10.1103/PhysRevD.96.063011). arXiv: [1707.03368](https://arxiv.org/abs/1707.03368). URL: <http://arxiv.org/abs/1707.03368> (visited on 07/01/2018).
- [26] Wolfgang Tichy and Bernd Bruegmann. “Quasi-equilibrium binary black hole sequences for puncture data derived from helical Killing vector conditions”. In: *Physical Review D* 69.2 (Jan. 22, 2004). ISSN: 1550-7998, 1550-2368. DOI: [10.1103/PhysRevD.69.024006](https://doi.org/10.1103/PhysRevD.69.024006). arXiv: [gr-qc / 0307027](https://arxiv.org/abs/gr-qc/0307027). URL: <http://arxiv.org/abs/gr-qc/0307027> (visited on 05/15/2018).
- [27] Marcus Ansorg, Bernd Brügmann, and Wolfgang Tichy. “A single-domain spectral method for black hole puncture data”. In: *Phys. Rev. D* 70 (2004), p. 064011. DOI: [10.1103/PhysRevD.70.064011](https://doi.org/10.1103/PhysRevD.70.064011). eprint: [arXiv:gr-qc/0404056](https://arxiv.org/abs/gr-qc/0404056).
- [28] J. David Brown et al. “Turduckening black holes: an analytical and computational study”. In: *Phys. Rev. D* 79 (2009), p. 044023. DOI: [10.1103/PhysRevD.79.044023](https://doi.org/10.1103/PhysRevD.79.044023). eprint: [arXiv:0809.3533\[gr-qc\]](https://arxiv.org/abs/0809.3533[gr-qc]).
- [29] *McLachlan, a Public BSSN Code*. URL: <http://www.eet.lsu.edu/~eschnett/McLachlan/>.
- [30] *Kranc: Kranc Assembles Numerical Code*. URL: <http://kranccode.org/>.
- [31] *LORENE: Langage Objet pour la R<sup>E</sup>lativit<sup>E</sup> Num<sup>E</sup>riquE*. URL: <http://www.lorene.obspm.fr/>.
- [32] Philipp Moesta et al. “GRHydro: A new open source general-relativistic magnetohydrodynamics code for the Einstein Toolkit”. In: *Classical and Quantum Gravity* 31.1 (Jan. 7, 2014), p. 015005. ISSN: 0264-9381, 1361-6382. DOI: [10.1088/0264-9381/31/1/015005](https://doi.org/10.1088/0264-9381/31/1/015005). arXiv: [1304.5544](https://arxiv.org/abs/1304.5544). URL: <http://arxiv.org/abs/1304.5544> (visited on 04/28/2018).
- [33] Masaru Shibata. “Simulation of merging binary neutron stars in full general relativity: 2 case”. In: *PHYSICAL REVIEW D* (), p. 18.
- [34] Kenta Kiuchi et al. “Long-term general relativistic simulation of binary neutron stars collapsing to a black hole”. In: *Physical Review D* 80.6 (Sept. 25, 2009). ISSN: 1550-7998, 1550-2368. DOI: [10.1103/PhysRevD.80.064037](https://doi.org/10.1103/PhysRevD.80.064037). URL: <https://link.aps.org/doi/10.1103/PhysRevD.80.064037> (visited on 04/18/2018).